An anti-silencer– and SATB1-dependent chromatin hub regulates *Rag1* and *Rag2* gene expression during thymocyte development

Bingtao Hao,[1] Abani Kanta Naik,[1] Akiko Watanabe,[1] Hirokazu Tanaka,[2] Liang Chen,[1] Hunter W. Richards,[3] Motonari Kondo,[1] Ichiro Taniuchi,[2] Yoshinori Kohwi,[3] Terumi Kohwi-Shigematsu,[3] and Michael S. Krangel[1]

[1]Department of Immunology, Duke University Medical Center, Durham, NC 27710
[2]RIKEN Centre for Integrative Medical Sciences, Yokohama, Kanagawa 230-0045, Japan
[3]Life Sciences Division, Lawrence Berkeley National Laboratory, University of California, Berkeley, Berkeley, CA 94720

***Rag1* and *Rag2* gene expression in CD4$^+$CD8$^+$ double-positive (DP) thymocytes depends on the activity of a distant anti-silencer element (ASE) that counteracts the activity of an intergenic silencer. However, the mechanistic basis for ASE activity is unknown. Here, we show that the ASE physically interacts with the distant *Rag1* and *Rag2* gene promoters in DP thymocytes, bringing the two promoters together to form an active chromatin hub. Moreover, we show that the ASE functions as a classical enhancer that can potently activate these promoters in the absence of the silencer or other locus elements. In thymocytes lacking the chromatin organizer SATB1, we identified a partial defect in *Tcra* gene rearrangement that was associated with reduced expression of *Rag1* and *Rag2* at the DP stage. SATB1 binds to the ASE and *Rag* promoters, facilitating inclusion of *Rag2* in the chromatin hub and the loading of RNA polymerase II to both the *Rag1* and *Rag2* promoters. Our results provide a novel framework for understanding ASE function and demonstrate a novel role for SATB1 as a regulator of *Rag* locus organization and gene expression in DP thymocytes.**

CORRESPONDENCE
Michael S. Krangel:
krang001@mc.duke.edu

Abbreviations used: 3C, chromosome conformation capture; ASE, anti-silencer element; BAC, bacterial artificial chromosome; ChIP, chromatin immunoprecipitation; ChIP-seq, ChIP-sequencing; DP, double positive; FAIRE, formaldehyde-assisted isolation of regulatory elements; H3K4me1, histone H3 lysine 4 monomethylation; H3K4me3, histone H3 lysine 4 trimethylation; H3K27ac, histone H3 lysine 27 acetylation; H3K27me3, histone H3 lysine 27 trimethylation; RAG, recombination activating gene; RNA Pol II, RNA polymerase II; RSS, recombination signal sequence; SATB1, special AT-rich binding protein 1; SP, single positive; V(D)J, variable, diversity, and joining gene segment.

The diverse antigen receptor repertoires of T and B lymphocytes are generated by a site-specific DNA recombination process that assembles antigen receptor variable (V), diversity (D), and joining (J) gene segments in developing lymphocytes. This process, known as V(D)J recombination, is initiated by a protein complex composed of recombination activating genes 1 and 2 (RAG1 and RAG2), which can recognize and cleave at recombination signal sequences (RSSs) that flank TCR and immunoglobulin V, D, and J gene segments (Schatz and Swanson, 2011). The *Rag1* and *Rag2* genes display a distinctive, tightly linked genomic organization with stringently and coordinately regulated expression during T and B lymphocyte development (Kuo and Schlissel, 2009).

There are two developmental windows of *Rag1* and *Rag2* (hereafter, *Rag*) gene expression during T and B lymphocyte development (Kuo and Schlissel, 2009). In developing thymocytes, the *Rag* genes are first expressed at the CD4$^-$CD8$^-$ double-negative (DN) stage to promote recombination of the *Tcrb*, *Tcrg*, and *Tcrd* genes. Productive *Tcrb* recombination causes *Rag* gene down-regulation, cellular proliferation, and differentiation to the CD4$^+$CD8$^+$ double-positive (DP) stage. *Rag* genes are then reexpressed in DP thymocytes to promote recombination of *Tcra* genes. After productive *Tcra* gene assembly and positive selection of TCR-expressing DP thymocytes, *Rag* genes are silenced during differentiation to the CD4$^+$CD8$^-$ or CD4$^-$CD8$^+$ single-positive (SP) stage. In similar fashion, an initial phase of *Rag* gene expression

B. Hao's present address is Dept. of Pathology, New York University School of Medicine, New York, NY 10016.
M. Kondo's present address is Dept. of Molecular Immunology, Toho University School of Medicine, Ota-ku, Tokyo 143-8540, Japan.

The Rockefeller University Press $30.00
J. Exp. Med. 2015 Vol. 212 No. 5 809–824
www.jem.org/cgi/doi/10.1084/jem.20142207

The Journal of Experimental Medicine

in prepro– and pro–B cells mediates recombination of *Igh* genes, whereas a subsequent phase of *Rag* gene expression in small pre–B cells mediates recombination of *Igk* and *Igl* genes.

Transcriptional regulation of the *Rag* genes is complex, involving distinct sets of lineage- and stage-specific cis-elements that cooperate with the *Rag1* and *Rag2* promoters (Kuo and Schlissel, 2009). *Rag* expression in developing B cells depends on sequences upstream of the *Rag2* promoter, including a proximal enhancer at −2.6 kb, a distal enhancer at −8 kb, and the well-studied Erag enhancer at −23 kb (Hsu et al., 2003; Kuo and Schlissel, 2009). Sequences within 10 kb of *Rag2* appear capable of supporting *Rag* gene expression in DN thymocytes (Monroe et al., 1999; Yu et al., 1999); however, in DP cells, *Rag* gene expression is critically dependent on a more distant element located between 71 and 79 kb upstream of *Rag2* (Yannoutsos et al., 2004). Elimination of this so-called anti-silencer element (ASE) by gene targeting reduced *Rag1* and *Rag2* expression by two orders of magnitude in DP thymocytes and prevented differentiation into SP cells, but had only modest effects on *Rag* gene expression in DN thymocytes (Yannoutsos et al., 2004). Studies with transgenic mice also revealed the presence of a silencer element between the *Rag1* and *Rag2* genes, which can extinguish *Rag* expression in DP thymocytes and partially suppress expression in DN thymocytes. Importantly, ASE activity was shown to be essential to counteract the suppressive effects of the intergenic silencer in DP thymocytes (Yannoutsos et al., 2004). Silencer activity depends on a binding site for *Runx* transcription factors, but further mechanistic information about ASE or silencer function has been lacking.

Gene regulation by distal elements generally depends on long range interactions that are facilitated by chromatin architectural proteins (Gibcus and Dekker, 2013; Merkenschlager and Odom, 2013). Special AT-rich binding protein 1 (SATB1) is a nuclear matrix/scaffold-associated DNA-binding protein that participates in the maintenance of chromatin architecture and regulates the expression of a large number of genes (Alvarez et al., 2000; Kumar et al., 2007; Han et al., 2008; Ahlfors et al., 2010). SATB1 binds ATC-rich DNA sequences (also referred to as base unpairing regions) and anchors these sequences to the nuclear matrix to form loops (Cai et al., 2003, 2006; Kumar et al., 2007). In addition, SATB1 can tether genes to the nuclear matrix by protein–protein interactions (Skowronska-Krawczyk et al., 2014). SATB1 can also recruit chromatin remodeling complexes that either promote or inhibit gene expression (Kumar et al., 2006). Given these activities, it is not surprising that SATB1 regulates gene expression programs in a wide variety of cells, including embryonal stem cells (Savarese et al., 2009), neuronal cells (Balamotis et al., 2012), epithelial progenitor cells (Fessing et al., 2011), pituitary cells (Skowronska-Krawczyk et al., 2014), and many tumors (Kohwi-Shigematsu et al., 2013). Within the hematopoietic compartment, SATB1 is expressed in stem cells and is then upregulated during their commitment to lymphoid lineages (Satoh et al., 2013; Will et al., 2013). In hematopoietic stem cells, SATB1 maintains quiescence and the potential for long-term self-renewal (Will et al., 2013). In hematopoietic progenitor cells, SATB1 supports the expression of genes critical for lymphocyte development and plays an important role in lymphopoiesis (Satoh et al., 2013). SATB1 is expressed at unusually high levels in the thymus (Dickinson et al., 1992), and *Satb1*-null mice display inefficient T cell development with the major block at the DP stage, resulting in dramatically reduced numbers of SP thymocytes and peripheral T cells (Alvarez et al., 2000; Satoh et al., 2013). SATB1 is also regulated in the context of peripheral T cell activation and differentiation (Cai et al., 2006; Lund et al., 2005), with increased expression required for Th2 differentiation and cytokine gene expression (Cai et al., 2006; Ahlfors et al., 2010; Notani et al., 2010). Conversely, reductions in SATB1 expression are critical for regulatory T cell function (Beyer et al., 2011).

Given the well-established role of chromosome architecture in regulating gene expression and assembly of antigen receptor loci (Jhunjhunwala et al., 2009; Shih and Krangel, 2013), we investigated whether SATB1 functions to regulate V(D)J recombination in DP thymocytes. We found that *Tcra* gene rearrangement is partially impaired in SATB1-deficient thymocytes, a defect that was associated with substantially reduced expression of *Rag1* and *Rag2* at the DP stage. Our analysis of this expression defect revealed that the ASE and *Rag* promoters interact over long-distances in DP thymocytes and that SATB1 is important to bring *Rag2* into this complex and to load RNA polymerase II (RNA pol II) to the *Rag1* and *Rag2* promoters. Our results provide a novel framework for understanding ASE function and the mechanistic basis for *Rag* gene expression in DP thymocytes.

RESULTS

Impaired *Tcra* rearrangement in SATB1-deficient DP thymocytes

To investigate its role in V(D)J recombination, we disrupted the gene encoding SATB1 in long-term hematopoietic stem cells of *Satb1*$^{f/f}$ mice (unpublished data) using a *Vav*-Cre transgene. Unlike *Satb1*-null mice (Alvarez et al., 2000), *Satb1*$^{f/f}$*Vav*-Cre mice displayed normal growth and survival. Total thymocyte numbers were reduced ∼60% in *Satb1*$^{f/f}$*Vav*-Cre as compared with *Satb1*$^{f/f}$ (also referred to as WT) mice, with similar reductions in the numbers of DN and DP thymocytes (Table 1 and Fig. S1). However, there were 85–90% reductions in SP thymocytes. Thus, *Satb1*-deficient thymocytes undergo a normal DN to DP transition, but an impaired transition from DP to SP. *Satb1* mRNA expression was reduced by ∼95% in DN3 thymocytes from *Satb1*$^{f/f}$*Vav*-Cre mice and its expression was essentially undetectable in DP thymocytes (Table 2).

We tested for V(D)J recombination defects using PCR to quantify *Tcra* locus Vα-to-Jα rearrangement in genomic DNA from WT and *Satb1*$^{f/f}$*Vav*-Cre thymocytes. The murine *Tcra/Tcrd* locus contains ∼100 Vα and 61 Jα gene segments which can undergo several rounds of recombination in DP thymocytes (Krangel, 2009). Newly generated DP thymocytes preferentially rearrange Vα segments to the most 5′ Jα

Table 1. Quantification of thymocyte subsets in WT (Satb1$^{fl/fl}$) and Satb1$^{-/-}$ (Satb1$^{f/f}$Vav-Cre) mice[a]

Cell population	WT (×10^{-5})	*Satb1*$^{-/-}$ (×10^{-5})
Total thymocytes (*n* = 6-7)	1,730 ± 610	670 ± 300[b]
DN1 (*n* = 3-4)	0.45 ± 0.30	0.20 ± 0.17
DN2 (*n* = 3-4)	0.89 ± 0.10	0.11 ± 0.10[c]
DN3 (*n* = 3-4)	17.9 ± 10.3	5.1 ± 3.4
CD8 ISP (*n* = 5-6)	22.0 ± 11.3	12.4 ± 9.1
DP (*n* = 6-7)	1,460 ± 500	570 ± 250[b]
CD4 SP (*n* = 6-7)	109 ± 49	17 ± 7[c]
CD8 SP (*n* = 6-7)	28.2 ± 11.6	2.7 ± 2.1[c]

[a]*Vav*-Cre transgenic mice have no intrinsic thymic phenotype (de Boer et al., 2003).
[b]$P < 0.01$ when compared with WT counterparts (Student's *t* test).
[c]$P < 0.001$ when compared with WT counterparts (Student's *t* test).

segments, whereas more mature DP thymocytes may replace these initial rearrangements by joining upstream Vα to more 3′ Jα segments. In *Satb1*$^{f/f}$*Vav*-Cre thymocytes, quantitative PCR revealed relatively normal Vα rearrangement to 5′ Jα segments, but impaired rearrangement to 3′ Jα segments (Fig. 1 A). This represented a deficiency in RAG-mediated cleavage at 3′ Jα gene segments rather than a deficiency in double-strand break repair, because similar reductions in signal end recombination intermediates at 3′ Jα gene segments were detected by ligation-mediated PCR (Fig. 1 B).

Defective 3′ Jα usage can result from impaired thymocyte survival (Guo et al., 2002). However, the survival of purified *Satb1*$^{f/f}$*Vav*-Cre DP thymocytes in culture was reduced only slightly as compared with WT thymocytes (Fig. 1 C). To further investigate a role for DP thymocyte viability in the Jα rearrangement defect, we introduced a *Bcl2* transgene into the *Satb1*$^{f/f}$*Vav*-Cre and WT backgrounds to extend thymocyte lifespan (Fig. 1 D). We then analyzed equal amounts of *Tcra* cDNA for 5′ and 3′ Jα segment usage. Consistent with the rearrangement defect noted above (Fig. 1, A and B), we observed a strong bias toward 5′ Jα usage in *Satb1*$^{f/f}$*Vav*-Cre as compared with WT thymocytes (Fig. 1 D; note that 5′ Jα usage in *Satb1*$^{f/f}$*Vav*-Cre thymocytes appears to be elevated over WT because Jα signals were normalized to total *Tcra* transcripts in this assay). The *Bcl2* transgene had minimal effect on the pattern of Jα usage in WT thymocytes; the notable exception was Jα2, where *Bcl2* expression appeared to protect from cell death those thymocytes that had exhausted the entire Jα array but failed to be positively selected. Although the *Bcl2* transgene partially ameliorated the strong bias toward 5′ Jα usage in *Satb1*$^{f/f}$*Vav*-Cre thymocytes, the 5′ bias nevertheless persisted and Jα usage in *Satb1*$^{f/f}$*Vav*-Cre *Bcl2* tg and *Satb1*$^{f/f}$ *Bcl2* tg thymocytes remained distinct. Thus, differential lifespan of DP thymocytes cannot account for differential Jα usage in SATB1-deficient and WT thymocytes. We also detected no change in germline transcription across the Jα-Cα region, suggesting that differential Jα usage does not reflect a change in Jα locus accessibility (Fig. 1 E).

Reduced *Rag1* and *Rag2* gene expression in SATB1-deficient DP thymocytes

Previous work had shown that impaired 3′ Jα usage can result from defective *Rag* gene expression in DP thymocytes (Yannoutsos et al., 2001). We therefore assessed *Rag1* and *Rag2* mRNA expression in DN and DP thymocytes from *Satb1*$^{f/f}$*Vav*-Cre and WT mice using real-time PCR (Fig. 2 A). Consistent with previous results (Yannoutsos et al., 2004) *Rag1* and *Rag2* expression were higher in DP thymocytes than in DN3 thymocytes from WT mice. SATB1-deficient thymocytes displayed normal *Rag1* and *Rag2* expression at the DN stage but displayed ∼70 and 80% reductions in *Rag1* and *Rag2* expression, respectively, in DP thymocytes. Similar reductions in *Rag1* and *Rag2* transcripts were observed in DP thymocytes from *Satb1*$^{f/f}$*Lck*-Cre mice; thus,

Table 2. Satb1 mRNA expression (relative to B2m) in thymocyte subsets of WT (Satb1$^{fl/fl}$) and Satb1$^{-/-}$ (Satb1$^{f/f}$Vav-Cre) mice[a]

SATB1/β2-microglobulin	WT (×10^{2})	*Satb1*$^{-/-}$ (×10^{2})
DN3 (*n* = 2)	3.28 ± 0.31	0.19 ± 0.02
DN4 (*n* = 2)	36.5 ± 2.68	0.13 ± 0.05
CD8 ISP (*n* = 2)	90.9 ± 40.8	ND[b]
DP (*n* = 2)	241 ± 51.5	0.0046 ± 0.0008
CD4 SP (*n* = 2)	26.4 ± 3.49	0.093 ± 0.041
CD8 SP (*n* = 2)	5.15 ± 0.30	0.0049 ± 0.0029

[a]RNA and cDNA were prepared from 30,000 cells.
[b]ND, not detected.

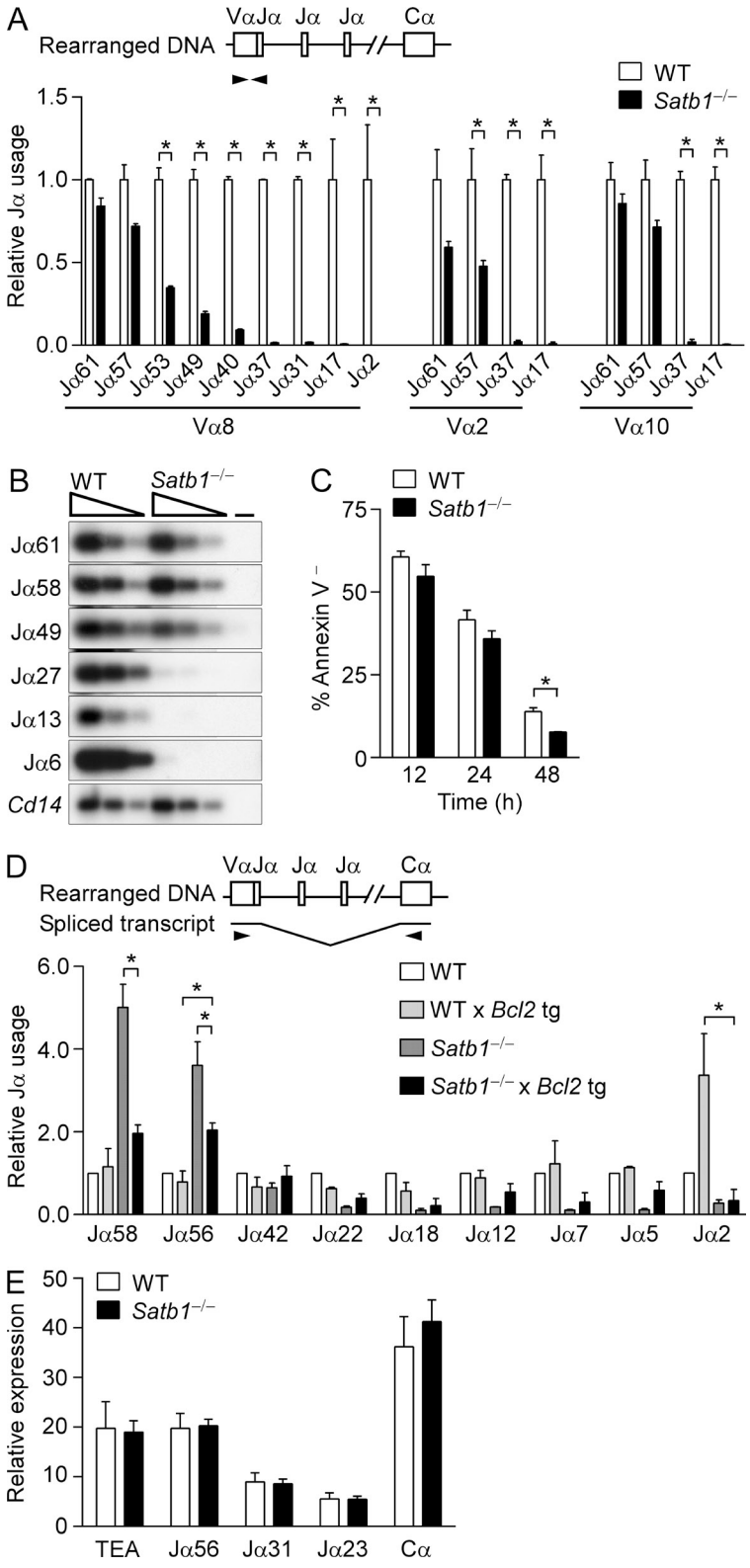

Figure 1. Defective *Tcra* rearrangement in SATB1-deficient thymocytes. (A) *Tcra* coding joints. Thymocyte genomic DNA samples were amplified by quantitative PCR using primers specific for the Vα8 (TRAV12), Vα2 (TRAV14), or Vα10 (TRAV13) families in conjunction with different Jα primers. The data are plotted as mean ± SEM of two experiments, each with one mouse per genotype, with values for SATB1-deficient thymocytes (*Satb1*$^{-/-}$, *Satb1*$^{f/f}$*Vav*-Cre) normalized to those for WT littermates (*Satb1*$^{f/f}$). *, P ≤ 0.05 by two-way ANOVA with Sidak's multiple comparisons test. (B) Jα signal ends. Three-fold serial dilutions of linker-ligated thymocyte genomic DNA samples were analyzed by PCR using Jα-specific and linker-primers. PCR products were visualized on Southern blots using radiolabeled Jα-specific oligonucleotide probes. The data are representative of two experiments, each with one mouse per genotype. −, no DNA. (C) DP thymocyte survival. WT and SATB1-deficient thymocytes were cultured in vitro for the indicated times and the percentage of Annexin V$^-$ DP thymocytes was determined. The data represent the mean ± SEM of two experiments, each with one mouse per genotype. *, P ≤ 0.05 by two-tailed Student's *t* test. (D) Relative Jα usage as a function of DP thymocyte lifespan. Vα8-Cα RT-PCR products were analyzed by Southern blot using radiolabeled Jα- and Cα-specific oligonucleotide probes. Relative Jα usage was evaluated by Phosphorimager as (Jα signal for [genotype]/Cα signal for [genotype])/(Jα signal for WT/Cα signal for WT). The data represent the mean ± SEM of two experiments, each with one mouse per genotype. *, P ≤ 0.05 by two-way ANOVA with Tukey's multiple comparisons test, comparing *Satb1*$^{-/-}$ *Bcl2* tg to WT *Bcl2* tg and *Satb1*$^{-/-}$. (E) *Tcra* germline transcription in SATB1-deficient thymocytes. WT (*Rag2*$^{-/-}$*Satb1*$^{f/f}$) and *Satb1*$^{-/-}$ (*Rag2*$^{-/-}$*Satb1*$^{f/f}$*Vav*-Cre) mice were injected with anti-CD3ε and total thymocytes were harvested 10 d later. Germline *Tcra* transcription was evaluated by quantitative RT-PCR. The data represent mean ± SEM of three experiments with WT and four experiments with *Satb1*$^{-/-}$ (one mouse per experiment), with normalization to values for *hprt*.

the *Rag* expression defect is T cell intrinsic (Fig. 2 B). Consistent with the reduced expression phenotype, chromatin immunoprecipitation (ChIP) revealed substantial reductions in the transcription-associated modification histone H3 lysine 4 trimethylation (H3K4me3) at the *Rag1* and *Rag2* promoters and gene bodies in *Satb1*$^{f/f}$*Vav*-Cre DP thymocytes (sites L, M, O and P, Fig. 2 C). We conclude that biased 5′ Jα usage in *Satb1*$^{f/f}$*Vav*-Cre thymocytes reflects inefficient

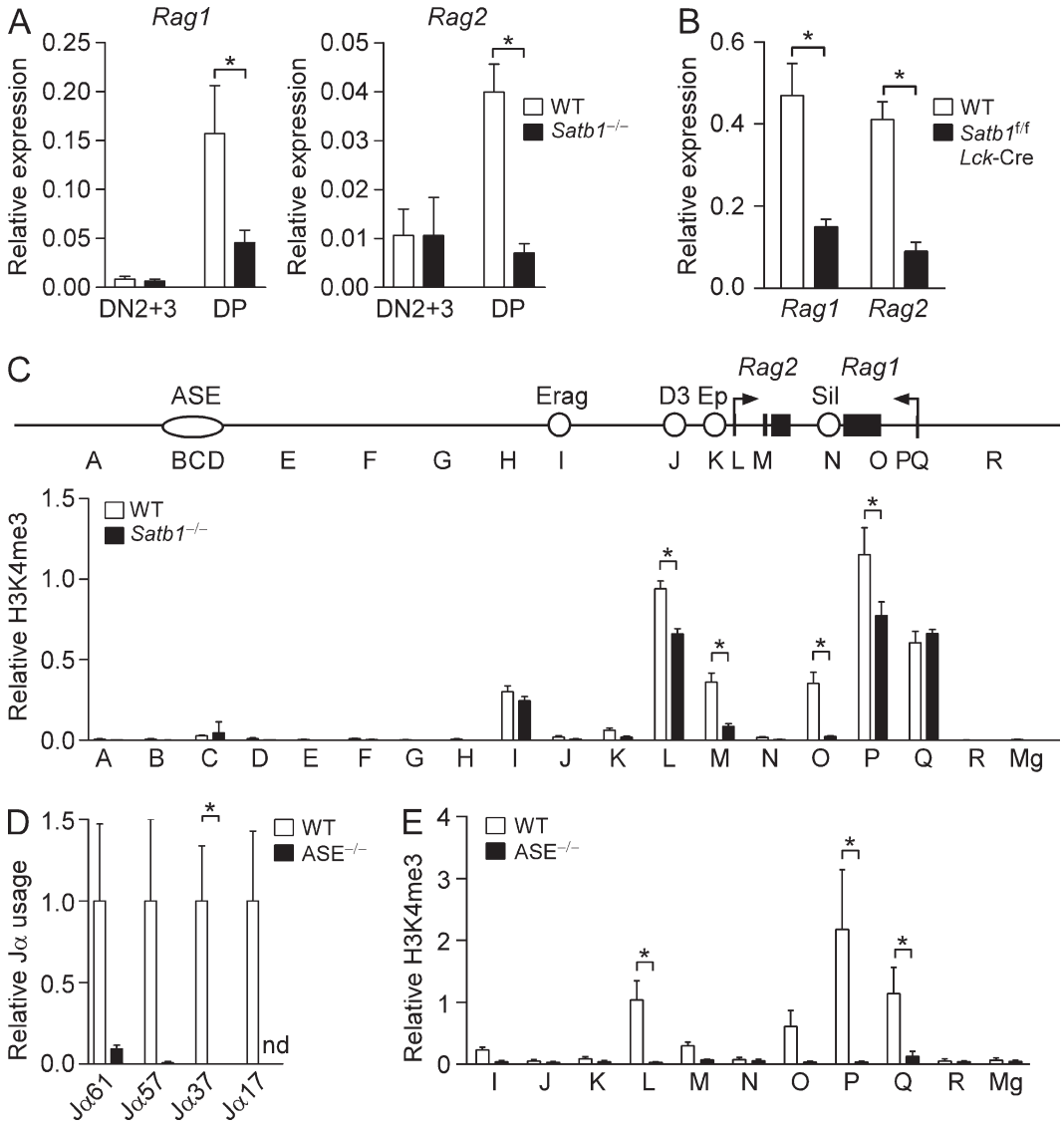

Figure 2. Defective *Rag*1 and *Rag2* gene expression in SATB1-deficient and ASE-deleted DP thymocytes. (A) The abundance of *Rag1* (left) and *Rag2* (right) transcripts in CD25+ (DN2+3) and DP thymocytes was evaluated by quantitative RT-PCR. The data represent the mean ± SEM of four experiments for DN2+3 and five experiments for DP (WT, *Satb1*$^{f/f}$; *Satb1*$^{-/-}$, *Satb1*$^{f/f}$*Vav*-Cre; one mouse per genotype per experiment) with normalization to values for *Actb*. *, P ≤ 0.05 by two-tailed Student's *t* test. (B) A T cell–intrinsic effect of SATB1 was evaluated by measuring transcript abundance in DP thymocytes of WT (*Satb1*$^{f/f}$) and *Satb1*$^{f/f}$*Lck*-Cre mice by quantitative RT-PCR. The data represent mean ± SEM of three experiments for WT and four experiments for *Satb1*$^{f/f}$*Lck*-Cre cDNA (one mouse per experiment), with normalization to values for *hprt*. *, P ≤ 0.05 by two-tailed Student's *t* test. (C) ChIP analysis of *Rag* locus histone H3K4me3. A map of the *Rag* locus depicts the convergently transcribed *Rag*1 and *Rag2* genes and known cis-regulatory elements ASE, Erag (enhancer of Rag), D3 (distal enhancer), Ep (enhancer proximal), and Sil (silencer; Kuo and Schlissel, 2009). Sorted DP thymocytes of WT and SATB1-deficient mice were analyzed by ChIP followed by quantitative PCR. Sites A–R in the *Rag* locus were analyzed by ChIP. The *MageA2* promoter (Mg) served as a negative control. The data represent the mean ± SEM of three experiments for each genotype (one mouse per experiment), with values of bound/input expressed relative to those for the *B2m* promoter (normalized to 1) in each sample. *, P ≤ 0.05 by two-way ANOVA with Sidak's multiple comparisons test. (D) *Tcra* coding joints in thymocytes of ASE-deleted mice. Thymocyte genomic DNA samples were amplified by quantitative PCR using a Vα8 family primer in conjunction with different Jα primers, with values for ASE$^{-/-}$ thymocytes normalized to those for WT littermates. The data represent the mean ± SEM of 2–3 independent preparations for each genotype. *, P ≤ 0.05 by two-tailed Student's *t* test. nd, not detected. (E) ChIP analysis of *Rag* locus histone H3K4me3 in DP thymocytes of ASE$^{-/-}$ mice. The data represent the mean ± SEM of four experiments for WT (ASE$^{+/+}$; one mouse per experiment) and five experiments for ASE$^{-/-}$ (one mouse per experiment). P ≤ 0.05 by two-way ANOVA with Sidak's multiple comparisons test.

rearrangement due to reduced *Rag* gene expression, and that this 5′ bias may be partially ameliorated by the *Bcl2* tg (Fig. 1 D) because thymocytes have additional time for rearrangements to occur.

Stage-specific and SATB1-dependent conformations of the *Rag* locus

Because *Satb1*$^{f/f}$*Vav*-Cre mice displayed a DP stage-specific defect in *Rag* gene expression, we hypothesized that SATB1

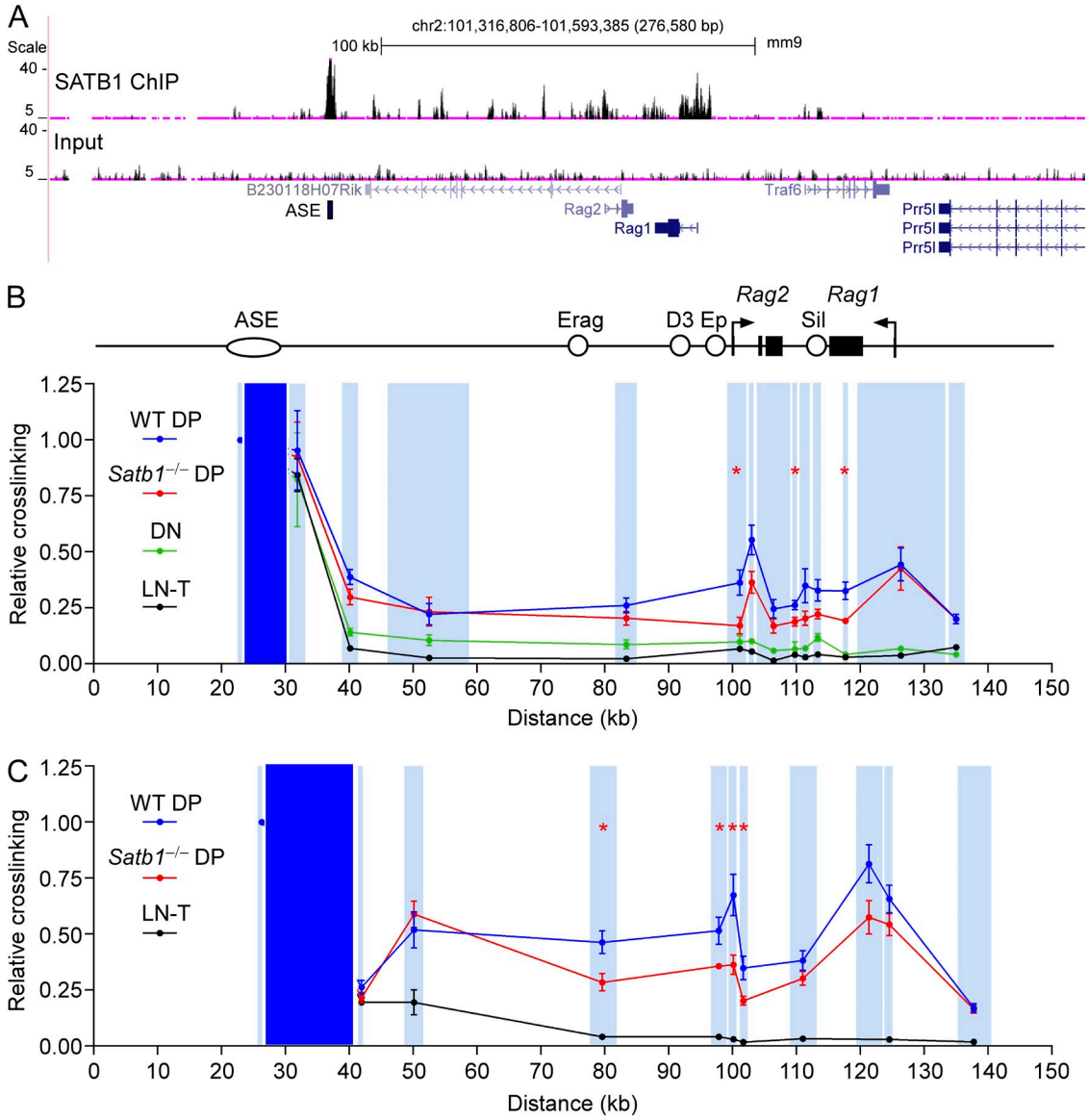

Figure 3. Developmentally regulated and SATB1-dependent interactions between the ASE and Rag promoters. (A) SATB1 ChIP-seq. Sequencing reads for SATB1 ChIP and input DNA are plotted. The ASE region marked corresponds to fragment AB (see Fig. 6). Long-distance interactions of the ASE-containing HindIII (B) or BglII (C) fragments were analyzed by 3C, followed by quantitative PCR. ASE viewpoint restriction fragments are shaded dark blue and target restriction fragments are shaded light blue. Primers were all reverse orientation and were positioned at the left end of each restriction fragment. Relative cross-linking data for each restriction fragment were plotted in the center of the fragment. Data in B represent mean ± SEM of two experiments with lymph node T cells (LN-T) cells (one mouse per experiment), three experiments with DN ($Lat^{-/-}$) thymocytes (one litter of five to eight mice per experiment), four experiments with WT ($Satb1^{f/f}$) DP thymocytes (one mouse per experiment), and four experiments with $Satb1^{-/-}$ ($Satb1^{f/f}$*Vav*-Cre) DP thymocytes (one mouse per experiment), all normalized to results for a nearest neighbor fragment (=1). *, P ≤ 0.05 by two-tailed Student's *t* test comparing WT to $Satb1^{-/-}$ DP. Data in C represent mean ± SEM of two experiments with LN-T cells (one mouse per experiment), eight experiments with WT DP thymocytes (one mouse per experiment), and six experiments with $Satb1^{-/-}$ DP thymocytes (one mouse per experiment), normalized as in B. *, P ≤ 0.05 by two-tailed Student's *t* test comparing WT to $Satb1^{-/-}$ DP.

might play a role in ASE function, perhaps by facilitating interactions between the ASE, 71-kb upstream of *Rag2*, and more proximal cis-acting elements. Prior analysis of $ASE^{-/-}$ mice revealed *Rag1* and *Rag2* gene expression to be <1% of the level in WT DP thymocytes (Yannoutsos et al., 2004), suggesting a more dramatic expression defect than in $Satb1^{f/f}$*Vav*-Cre mice. In accord with this, we found that $ASE^{-/-}$ DP thymocytes displayed more dramatic reductions in Vα-to-Jα recombination (Fig. 2 D) and in histone H3 lysine 4 trimethylation (H3K4me3) (Fig. 2 E) than in $Satb1^{f/f}$*Vav*-Cre mice. On this basis, we predicted that ASE functions and interactions might be partially diminished in

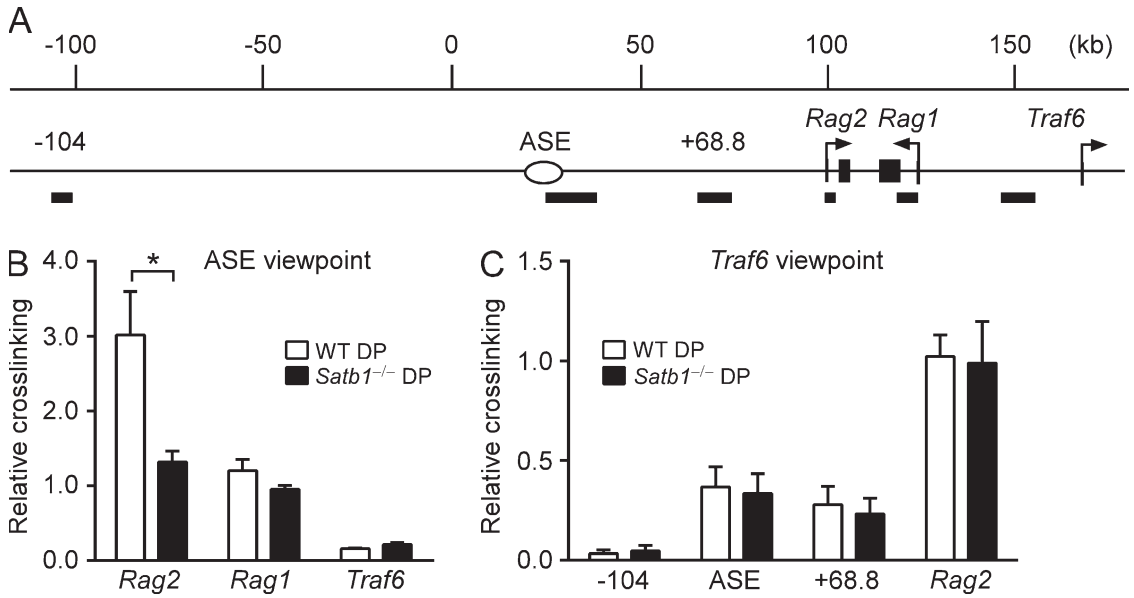

Figure 4. SATB1 specifically influences the ASE–Rag2 promoter interaction. (A) *Rag* locus map including flanking regions, with numbering concordant with Fig. 3. -104, ASE (+33.6), +68.8, *Rag2* (+100), *Rag1* (+121.2), and Traf6 (+151) identify the midpoints of BglII fragments (solid bars) chosen for 3C. Long-distance interactions of the ASE (B) or *Traf6* promoter (C) fragments were analyzed by 3C followed by quantitative PCR. Data represent mean ± SEM of four experiments with WT (*Satb1*$^{f/f}$) DP thymocytes (one mouse per experiment) and five experiments with *Satb1*$^{-/-}$ (*Satb1*$^{f/f}$*Vav*-Cre) DP thymocytes (one mouse per experiment), all normalized to results for the *Traf6* nearest neighbor fragment (=1). *, P ≤ 0.0001 by two-way ANOVA with Sidak's multiple comparisons test.

Satb1$^{f/f}$*Vav*-Cre mice. Consistent with such a role, ChIP-sequencing (ChIP-seq) analysis revealed prominent SATB1 binding to the ASE, as well as to the *Rag1* and *Rag2* promoter regions in DP thymocytes (Fig. 3 A).

Previous studies showed that the ASE is required to counteract functions of the *Rag* silencer; however, the mechanistic basis for this process remained uncertain (Yannoutsos et al., 2004). In this regard, the ASE could be envisioned to promote *Rag* gene expression as a consequence of direct physical interaction with the silencer in DP thymocytes. Alternatively, the ASE might counteract the influence of the silencer by interacting directly with the *Rag* gene promoters.

To investigate *Rag* locus architecture, we explored interactions between the ASE and *Rag* genes using chromosome conformation capture (3C; Dekker et al., 2002). In this approach, long-distance interactions in nuclei are initially captured by formaldehyde cross-linking; after restriction enzyme digestion, dilution, and intermolecular ligation, interacting DNA fragments are detected by real-time PCR. Using the ASE-containing HindIII fragment as a viewpoint, in WT DP thymocytes we detected interactions with HindIII fragments carrying the *Rag1* and *Rag2* promoters 70–100 kb away (Fig. 3 B). Similar ASE-*Rag* promoter interactions were detected between the relevant BglII fragments as well (Fig. 3 C). These interactions were specific, because they were not detected in LN T cells, which do not express the *Rag* genes. We evaluated chromatin interactions in the DN compartment by analyzing thymocytes from LAT-deficient mice, which are blocked at the DN stage of development (Zhang et al., 1999). Interaction frequencies were only slightly higher than in LN T cells (Fig. 3 B), consistent with a limited role for the ASE in *Rag* gene expression in DN thymocytes (Yannoutsos et al., 2004).

Notably, ASE interactions with the *Rag2* promoter were significantly attenuated in *Satb1*$^{f/f}$*Vav*-Cre DP thymocytes (Fig. 3, B and C). However, ASE-*Rag1* promoter contacts were either maintained (Fig. 3 B) or marginally reduced in a manner that did not reach statistical significance (Fig. 3 C). To address this point further, we analyzed an independent set of BglII-digested 3C samples and confirmed reduced ASE–*Rag2* promoter interaction but normal ASE–*Rag1* promoter interaction in *Satb1*$^{f/f}$*Vav*-Cre DP thymocytes (Fig. 4, A and B). Moreover, the requirement for SATB1 to facilitate ASE-*Rag2* promoter interaction was highly specific, because *Rag2* promoter contacts with the *Traf6* promoter were maintained in SATB1-deficient mice (Fig. 4, A and C). Although the *Rag2–Traf6* interaction serves as a useful control, it is of unknown biological significance.

Our 3C data indicated that, in addition to the *Rag* promoters, the ASE interacts broadly across the *Rag* locus (above the background in LN T cells), including sites between the ASE and *Rag2*, and within the *Rag2* and *Rag1* gene bodies (Fig. 3, B and C). Although the ASE contacts the region that includes the intergenic *Rag* silencer, these interactions were not elevated above the general levels observed across the *Rag* locus. Collectively, these data support a model in which the ASE indirectly counteracts silencer activity via direct interactions with the *Rag1* and *Rag2* promoters.

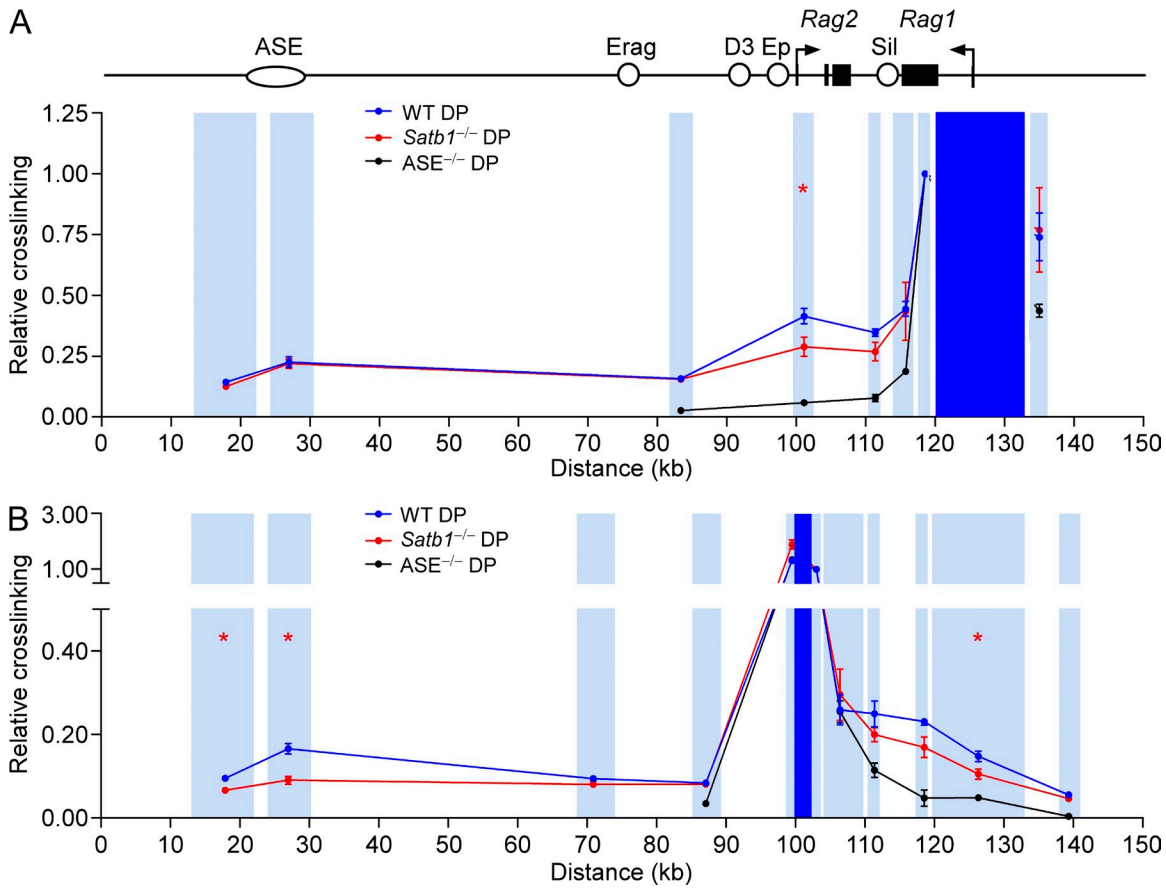

Figure 5. ASE- and SATB1-dependent interactions between the *Rag1* and *Rag2* promoters. Long-distance interactions of *Rag1* promoter-containing (A) or *Rag2* promoter-containing (B) HindIII fragments were analyzed by 3C followed by quantitative PCR. The *Rag1* promoter viewpoint (A) and Rag2 promoter viewpoint (B) restrictions fragments are shaded dark blue and target restriction fragments are shaded light blue. Primers for (A) were all reverse orientation and were positioned at the left end of each restriction fragment. Those for B were all forward orientation and were positioned at the right end of each restriction fragment. Relative cross-linking data for each restriction fragment were plotted in the center of the fragment. Data represent mean ± SEM of four experiments each for WT, *Satb1*$^{-/-}$ (*Satb1*$^{f/f}$ *Vav*-Cre), and ASE$^{-/-}$ DP thymocytes (one mouse per genotype per experiment), all normalized to results for a nearest neighbor fragment (=1). *, P ≤ 0.05 by two-tailed Student's *t* test comparing WT to *Satb1*$^{-/-}$ DP.

The ASE organizes the *Rag* locus

To further explore the role of the ASE in *Rag* locus conformation, we used 3C to assess long distance interactions in DP thymocytes from ASE$^{-/-}$ mice. Using the *Rag1* promoter fragment as a viewpoint, we detected an interaction between the *Rag1* and *Rag2* promoters in WT DP thymocytes and found this interaction to be substantially diminished in ASE$^{-/-}$ DP thymocytes (Fig. 5 A). Similar results were obtained using a *Rag2* promoter-containing fragment as the viewpoint (Fig. 5 B). Moreover, *Rag1–Rag2* promoter interactions were reduced partially in *Satb1*$^{f/f}$*Vav*-Cre DP thymocytes (Fig. 5, A and B). Using these new viewpoints, we also confirmed reduced interactions of the *Rag2* but not the *Rag1* promoter with the ASE in *Satb1*$^{f/f}$*Vav*-Cre DP thymocytes (Fig. 5, A and B), a finding consistent with 3C analyses from the ASE viewpoint (Figs. 3 and 4). We conclude that the ASE organizes the *Rag* locus by tethering the *Rag1* and *Rag2* promoters in DP thymocytes, and that efficient tethering of the *Rag2* promoter depends on SATB1.

The ASE is required for RNA pol II occupancy at the *Rag* promoters

To explore the functional significance of the DP-specific chromatin conformation of the *Rag* locus, we analyzed the RNA pol II distribution using ChIP. As anticipated, RNA pol II occupancy was high at the *Rag1* and *Rag2* promoters in WT DP thymocytes (sites L and Q, Fig. 6 A). However, RNA pol II was prominent at the ASE and silencer as well (sites C and N, Fig. 6 A). In DN thymocytes from *Lat*$^{-/-}$ mice, lower levels of RNA pol II were present at the *Rag* promoters and silencer, but at the ASE, RNA pol II was as abundant as in DP thymocytes. In contrast, RNA pol II was minimal at all sites in LN T cells (Fig. 6 A) and in ASE$^{-/-}$ DP thymocytes (Fig. 6 B). Thus, RNA pol II occupancy at the *Rag* promoters and silencer is developmentally regulated in a manner that correlates with transcription and depends on the ASE. A previous study also identified substantial RNA pol II binding to the *Rag* promoters, ASE, and silencer in DP thymocytes, although other stages of T cell development were not examined (Koch et al., 2011).

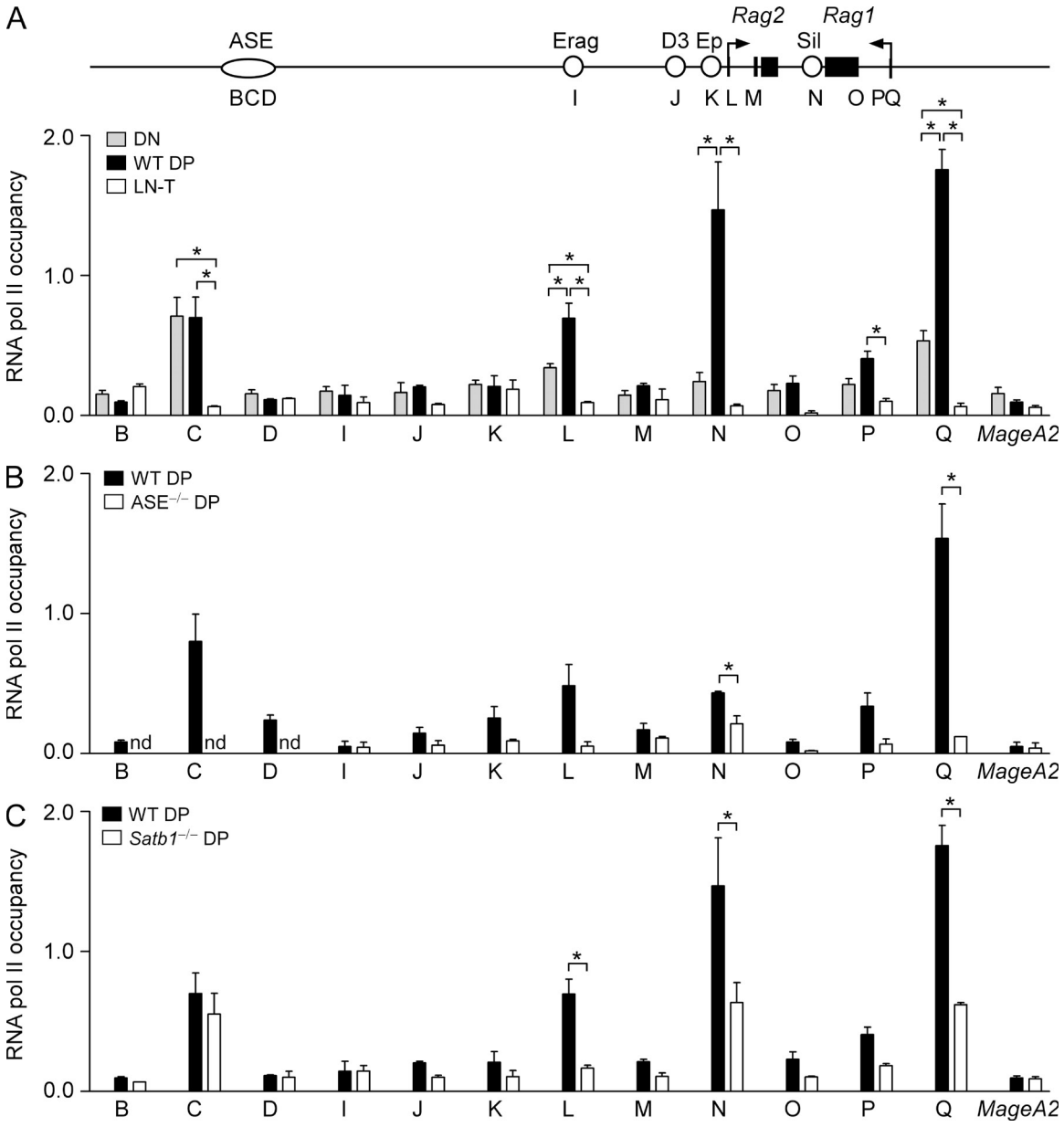

Figure 6. Locus conformation–dependent RNA pol II occupancy of the *Rag1* and *Rag2* promoters. RNA pol II occupancy was assessed by ChIP and quantitative PCR at sites spanning the Rag locus. Values of bound/input were expressed relative to those for *B2m* (normalized to 1) in each sample. *MageA2* served as a negative control. (A) Data represent mean ± SEM of three experiments each for DN (*Lat*$^{-/-}$) thymocytes (one litter of five to eight mice per experiment), WT DP (*Satb1*$^{f/f}$) thymocytes (one mouse per experiment), and lymph node T cells (LN-T; one mouse per experiment). Data for these three genotypes and *Satb1*$^{-/-}$ (*Satb1*$^{f/f}$*Vav*-Cre) DP thymocytes (three experiments, one mouse per experiment) were analyzed together by two way ANOVA with Tukey's multiple comparisons test, with the data for WT DP and *Satb1*$^{-/-}$ DP plotted separately in C. *, $P \leq 0.05$. (B) Data represent the mean ± SEM of three experiments for WT (ASE$^{+/+}$) DP thymocytes (one mouse per experiment) and two experiments for ASE$^{-/-}$ DP thymocytes (one mouse per experiment). *, $P \leq 0.05$ by two-tailed Student's *t* test. (C) Data represent the mean ± SEM of three experiments each for WT (*Satb1*$^{f/f}$; identical to A) DP thymocytes (one mouse per experiment) and *Satb1*$^{-/-}$ (*Satb1*$^{f/f}$*Vav*-Cre) DP thymocytes (one mouse per experiment). *, $P \leq 0.05$ by two-way ANOVA with Tukey's multiple comparisons test, as noted above. Samples in A and C were all analyzed in the same series of experiments; samples in B were analyzed separately.

Notably, RNA pol II occupancy at the *Rag* promoters and silencer was partially reduced in DP thymocytes from *Satb1*$^{f/f}$*Vav*-Cre mice, whereas occupancy at the ASE was unaffected (Fig. 6 C). Thus, RNA pol II occupancy at the ASE occurs independent of ASE–promoter interactions, whereas RNA pol II occupancy at the promoters and silencer correlates with assembly of an intact complex containing the ASE and the *Rag1* and *Rag2* promoters. Similarly, DN thymocytes display RNA pol II at the ASE but, in the absence of ASE–promoter interactions, only low levels at the *Rag* genes themselves (Fig. 6 A). We suggest that the *Rag1* and *Rag2* promoters acquire high levels of RNA pol II when they are tethered to

each other and to the ASE. Whether this reflects delivery of RNA pol II previously bound to the ASE or newly recruited RNA pol II remains an open question.

The ASE directly activates the *Rag1* and *Rag2* promoters

The above data imply that the ASE stimulates *Rag* gene transcription through direct long distance interactions with the *Rag1* and *Rag2* promoters, perhaps functioning as a classical enhancer. To test this possibility, we sought to define an ASE fragment that activates *Rag1* and *Rag2* promoter-driven luciferase reporter constructs in transiently transfected cells. Because previous work had only ascribed ASE activity to a broad 8-kb region (Yannoutsos et al., 2004), we asked whether a smaller core ASE possessed functional activity. Initially, we leveraged chromatin data from the mouse ENCODE database (Stamatoyannopoulos et al., 2012; Rosenbloom et al., 2013) to narrow our search. DNase-Seq data from unsorted thymocytes reveals a tightly linked pair of strong DNase I hypersensitive sites that span ∼2-kb and correspond to a previously identified region notable for substantial interspecies sequence conservation (Fig. 7 A; Yannoutsos et al., 2004). We further mapped open chromatin in the *Rag* locus in purified DP thymocytes using formaldehyde-assisted isolation of regulatory elements (FAIRE; Giresi et al., 2007), which similarly detected a 2-kb open chromatin region (Fig. 7 B). ENCODE data show that the same region harbors the characteristic chromatin signature of active enhancers in thymus but not in spleen: high histone H3 lysine 4 monomethylation (H3K4me1) and histone H3 lysine 27 acetylation (H3K27ac) coupled with low H3K4me3 and histone H3 lysine 27 trimethylation (Fig. 7 A; Bulger and Groudine, 2011; Natoli and Andrau, 2012; Calo and Wysocka, 2013). Moreover, our ChIP-seq data mapped SATB1 binding to the same region and, consistent with our ChIP data (Fig. 6 A), the region displayed high RNA pol II occupancy as well (Fig. 7 A).

We tested enhancer activity of the 2.0-kb ASE fragment that corresponded to the region of DNase I hypersensitivity and sequence conservation, as well as a 1.3-kb subfragment (AB) corresponding to the region of highest H3K4me1, H3K27ac, and RNA pol II. These test fragments were introduced into promoter-driven luciferase reporters that were transiently transfected into the murine DP thymocyte cell line VL3-3M2 (Fig. 7 C). By themselves, the *Rag1* and *Rag2* promoters drove minimal luciferase expression compared with positive control plasmids containing the promoters plus the *Tcr*a enhancer (Eα), a potent enhancer in DP thymocytes. Notably, the 2-kb ASE fragment and subfragment AB were more potent than Eα as activators of both promoters. To determine the minimal region responsible for enhancer activity, we tested two partially overlapping subfragments of AB (fragments A and B). Both displayed enhancer activity, with the activity of the 2-kb ASE or fragment AB only marginally better than either A or B. This suggested that the 140-bp region shared by fragments A and B, which is centered within the strong peaks of H3K4me1, H3K27ac, RNA pol II, and SATB1, might play a dominant role in enhancer activity. Indeed, fragments A' and B', truncated versions of A and B lacking the 140-bp overlap region, displayed no detectable enhancer activity, whereas the 140-bp overlap region exhibited enhancer function comparable to that of Eα. We conclude that the 140-bp ASE fragment, which contains evolutionarily conserved binding sites for E2A-, Runx-, GATA-, and Ikaros-family transcription factors (Fig. 7 D), is a core enhancer element that augments the function of the *Rag* promoters. However, because activity of the 140-bp fragment was substantially reduced relative to larger ASE fragments, flanking sequences are likely to boost enhancer activity even further.

DISCUSSION

The Rag silencer and ASE were previously shown to coordinate *Rag* gene expression in DP thymocytes (Yannoutsos et al., 2004). The silencer was defined using bacterial artificial chromosome (BAC) reporter transgenes lacking the ASE. In such constructs, silencer deletion caused increases in *Rag* gene expression in DN and DP thymocytes but not in developing B cells. Moreover, the silencer could suppress the expression of a heterologous reporter transgene in pre–B cells, DN and DP thymocytes, and splenic T cells. Thus, the silencer appeared to be capable of broadly suppressing the activities of linked promoters in lymphoid cells. In BAC constructs containing the intergenic silencer, the ASE was shown to be required for *Rag* expression in DP thymocytes and to increase *Rag* expression in DN3 thymocytes. However, it had no apparent effect on *Rag* expression in constructs lacking the silencer. Consistent with these observations, gene-targeted deletion of the ASE reduced *Rag* expression in DN thymocytes, abrogated *Rag* expression in DP thymocytes, and caused a developmental block at the DP stage that was likely secondary to impaired *Tcra* gene recombination. Thus, ASE activity was strongest in DP thymocytes, but the ASE was judged to be distinct from a classical enhancer because it appeared to function by counteracting the activity of an intergenic silencer (Yannoutsos et al., 2004).

These foundational studies left the mechanistic basis for ASE activity unclear. As one possibility, the ASE could functionally interact with the silencer to neutralize its ability to suppress the *Rag* promoters. Alternatively, the ASE could functionally interact with the *Rag* promoters to overcome the suppressive effects of the silencer. Our data strongly support the latter scenario and argue that the ASE functions as a classical enhancer: it displays a chromatin signature typical of active enhancers, it interacts physically with the distant *Rag1* and *Rag2* promoters and brings these promoters together to form a chromatin hub in DP thymocytes (Fig. 8), and it can directly and potently activate the *Rag1* and *Rag2* promoters in the absence of the silencer or any other locus elements.

Our data yield a picture that diverges in two respects from the initial description of ASE activity. First, the chromosomal BAC reporter studies identified no ASE activity in constructs lacking the silencer (Yannoutsos et al., 2004), whereas we show that the ASE can function as a direct activator of the *Rag1* and *Rag2* promoters in extrachromosomal luciferase

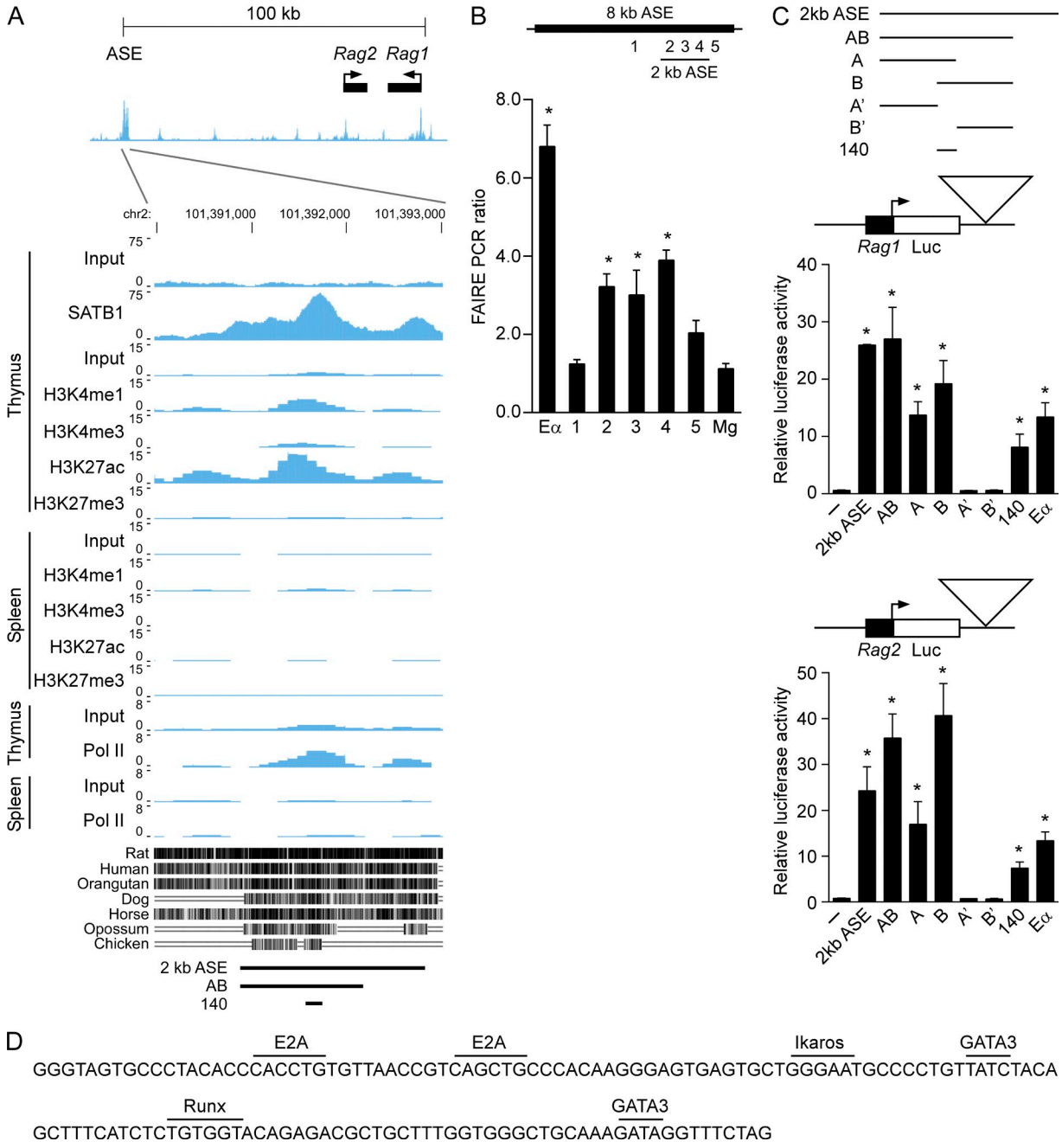

Figure 7. The ASE directly activates the *Rag1* and *Rag2* promoters. (A) ENCODE data tracks in the Mouse July 2007 (NCBI37/mm9) assembly are shown. (top) DNase-seq data for the *Rag* locus in unfractionated thymocytes. (bottom) ChIP-Seq data and sequence conservation for the DNase hypersensitive region in unfractionated thymocytes and splenocytes. Note that primer sets B and D (Fig. 6) map upstream and downstream, respectively, of the 2-kb open chromatin region whereas primer set C maps within the 140-bp minimal enhancer region. (B) FAIRE samples were prepared to evaluate open chromatin at the ASE in WT DP thymocytes. Quantitative PCR was used to evaluate enrichment of sequences in DNA purified from formaldehyde-cross-linked as compared with uncrosslinked samples. The *Tcra* enhancer (Eα) and *MageA2* (Mg) served as positive and negative controls, respectively. Positions of test amplicons relative to the 8-kb ASE region are indicated above the graph. The data are presented as mean ± SEM of values of cross-linked/uncrosslinked in three experiments (one mouse per experiment). *, $P \leq 0.05$ by two-tailed Student's *t* test comparing Eα and test amplicons to *MageA2*. (C) ASE activation of the *Rag1* and *Rag2* promoters. Test ASE fragments were cloned downstream of either a *Rag1* promoter-driven or a *Rag2* promoter-driven luciferase gene and were assayed by transient transfection into VL3-3M2 DP thymocytes. The data represent the mean ± SEM of two to four independent experiments. *, $P \leq 0.05$ by two-tailed Student's *t* test comparing results for test ASE fragments to promoter-only controls (−). (D) Nucleotide sequence of the 140-bp minimal enhancer with predicted binding sites for transcription factors marked.

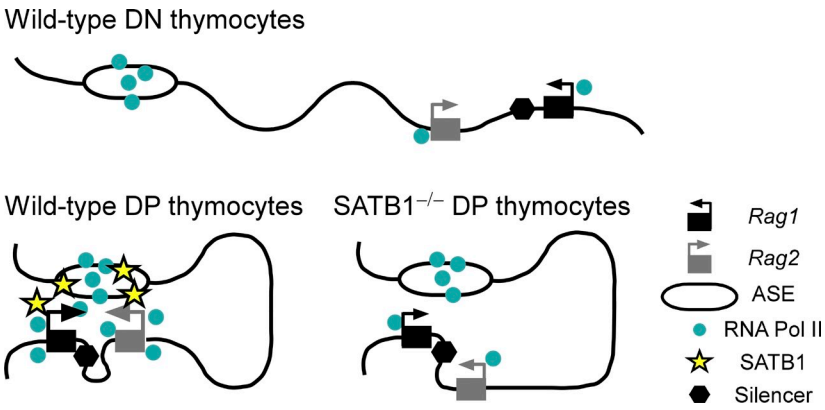

Figure 8. Model depicting ASE- and SATB1-dependent Rag1 and Rag2 gene expression in DP thymocytes. The *Rag1* and *Rag2* promoters have minimal contact with the RNA polII-loaded ASE in DN thymocytes and are transcribed at modest levels. SATB1 is up-regulated in DP thymocytes, binds to the ASE and *Rag* promoters, and facilitates formation of a chromatin hub that promotes RNA Pol II recruitment and trans-activation of the promoters. In the absence of SATB1, the *Rag2* promoter is preferentially excluded from the chromatin hub, leading to reduced RNA Pol II recruitment and trans-activation of both promoters.

reporters that lack the silencer. One explanation for this difference could be that the analysis of a small number of BAC integrants did not provide an accurate picture of ASE activity. However, we favor an alternate possibility: in the environment of a chromosomally integrated locus, the silencer may be essential to create a repressive environment at the promoters that would enforce the need for ASE activity, whereas extrachromosomal reporters may be intrinsically suppressed at the promoters even in the absence of the silencer. A second point of divergence is that the BAC reporter studies showed the ASE to be active but not essential for *Rag* gene expression in DN thymocytes, whereas we see no clear evidence for long-distance interaction between the ASE and the *Rag* promoters in that compartment. This difference may simply reflect insensitivity of our 3C analysis to low frequency ASE–promoter interactions that may occur in DN thymocytes. Nevertheless, the BAC transgene and our current work are concordant in many regards, especially the greater reliance on ASE activity and long-distance interactions in DP compared with DN thymocytes.

The intriguing distribution of RNA pol II at the Rag locus suggests potential mechanisms by which the ASE might regulate *Rag* gene expression. At the ASE, we found RNA pol II to be present at high levels in DN and DP thymocytes and in SATB1-deficient DP thymocytes, but not in LN T cells. However, high level RNA pol II occupancy at the *Rag1* and *Rag2* promoters was only detected in SATB1-sufficient DP thymocytes, thereby correlating with looping between the ASE and the two *Rag* promoters. This suggests that an important function of these regulatory loops is to promote RNA pol II loading to the promoters (Fig. 8). RNA pol II binding is a shared property of many enhancers and is often associated with the transcription of enhancer RNAs (Kim et al., 2010; Koch et al., 2011; Natoli and Andrau, 2012). Recent data suggest that enhancer RNAs may play a direct role in enhancer-promoter looping and promoter activation via a mechanism that may involve cohesin (Li et al., 2013). Consistent with these possibilities, the ASE binds TATA-binding protein and general transcription factors in addition to RNA pol II (Koch et al., 2011), and there is low-level ASE transcription in DP thymocytes. RNA pol II initially recruited to the ASE could be delivered to the *Rag* promoters as a consequence of ASE–promoter interactions. Alternatively, ASE–promoter interactions could stabilize the binding of newly recruited RNA pol II at the *Rag* promoters. Viewed in another way, the ASE may frequently localize to a transcription factor (Cisse et al., 2013; Cook, 1999; Ghamari et al., 2013) in DN and DP thymocytes, and ASE–promoter interactions and elevated promoter RNA pol II occupancy may reflect high frequency recruitment of the *Rag* promoters into the same transcription factory in DP thymocytes. The substantially reduced *Rag* transcription that occurs in DN thymocytes may then be interpreted as a reduced frequency of promoter recruitment to ASE-containing transcription factories in these cells.

RNA pol II was also detected in the *Rag* silencer region. This binding had a profile similar to that of the *Rag* promoters, in that it was elevated in DP thymocytes in an ASE- and SATB1-dependent manner, thereby correlating with long-distance looping and high levels of *Rag* gene transcription. Of note, RNA pol II occupancy maps to the very 3′ end of the *Rag1* transcription unit (Rosenbloom et al., 2013; Stamatoyannopoulos et al., 2012), ∼700 bp away from the Runx binding-site that was shown to be essential for silencer activity (Yannoutsos et al., 2004). Moreover, this RNA pol II is primarily in the serine 2 phosphorylated form (Koch et al., 2011). Based on this, we suspect that the accumulation of RNA pol II at this site is related to the termination of *Rag1* transcription and not to silencer function.

Finally, our data suggest important roles for chromatin organizer SATB1 in *Rag* gene expression and *Tcra* recombination in DP thymocytes. SATB1 expression is dramatically up-regulated in DP thymocytes (Table 2), correlating with the substantial increases in *Rag* gene expression in this compartment. Further, SATB1 binds to multiple sites across the *Rag* locus, most prominently at the ASE and *Rag1* and *Rag2* promoters. We suspect that SATB1 binding to the *Rag* locus is up-regulated in parallel with its increased expression in DP thymocytes, although our experiments do not directly address this point. However, loss of SATB1 led to significant reductions in *Rag* gene expression, in *Rag2* promoter interactions with the ASE and *Rag1* promoter, and in RNA pol II occupancy at the *Rag* promoters and silencer in DP thymocytes

(Fig. 8). Thus, our results for the *Rag* locus are fully consistent with prior examples in which SATB1 was shown to regulate genomic loci by tethering the bases of chromatin loops and recruiting critical chromatin remodeling complexes and RNA Pol II (Cai et al., 2003, 2006; Kumar et al., 2007). Our results indicate that ASE–*Rag1* promoter interactions can be assembled in a SATB1-independent fashion, but that the *Rag2* promoter depends on SATB1 to effectively join this complex (Fig. 8). Reduced RNA pol II loading and transcription of *Rag2* in the absence of SATB1 may be a straightforward consequence of exclusion of this promoter from the ASE-*Rag1* complex. However, RNA pol II loading and transcription of *Rag1* are also reduced in the absence of SATB1 even though the *Rag1* promoter maintains contact with the ASE. This suggests that *Rag1* promoter activity may depend on the formation of a holocomplex containing the ASE and both promoters. Alternatively, SATB1 could play a more direct role in ASE or promoter activity in addition to mediating their long-distance interactions. Consistent with this possibility, SATB1 binding is centered within the 140-bp enhancer core of the ASE.

In summary, we demonstrate that *Rag* gene expression in DP thymocytes depends on the assembly of a multi-component chromatin complex, or hub, containing the ASE and both *Rag* gene promoters. We show, too, that chromatin organizer SATB1 plays an important role in the assembly of this complex and in *Rag* gene transcription, functioning at least in part by stimulating RNA pol II loading to the *Rag* promoters. Whether SATB1 serves purely in an architectural capacity to facilitate long-distance looping, or also functions in a more direct manner to effect promoter activation, will be an important issue for future studies.

MATERIALS AND METHODS

Mice. ASE$^{-/-}$ mice (Yannoutsos et al., 2004) and *Vav*-Cre mice (de Boer et al., 2003) were obtained from The Jackson Laboratory. *Bcl2* transgenic mice (Domen et al., 1998) and *Lat*$^{-/-}$ mice (Zhang et al., 1999) were provided by J. Domen (Duke University, Durham, NC) and W. Zhang (Duke University, Durham, NC), respectively. Mice were maintained on a C57BL/6 background and were housed in specific pathogen-free conditions. All mice were used in accordance with protocols approved by the Duke University Institutional Animal Care and Use Committee.

Flow cytometry and cell sorting. For surface staining, erythrocyte-lysed single-cell suspensions were prepared in staining medium (DMEM + 2% FCS) with 1 mg/ml normal rat IgG (Sigma-Aldrich) and were stained on ice for 20 min using the following antibodies: FITC-CD8α (53–6.7), PE-CD3ε (145-2C11), PE/Cy5-B220 (RA3-6B2), Mac-1 (M1/70), Gr-1 (RB6-8C5), TER119 (TER-119), PE/Cy7-CD4 (GK1.5), APC-CD44 (IM7), TCRβ (H57-597), and APC/Cy7-CD25 (PC61.5) from eBioscience, as well as PE/Cy5-CD11c (HL3) from BD. FACS analyses were performed on a FACSCanto II (BD) and data were analyzed with FlowJo software (Tree Star).

For cell sorting, single-cell suspensions were prepared following erythrocyte lysis. DN3 thymocytes (CD4$^-$CD8$^-$CD25$^+$CD44$^{-/lo}$) and a combined DN2/3 thymocyte population (CD4$^-$CD8$^-$CD25$^+$) were obtained after initial depletion of CD4$^+$ and CD8$^+$ cells using biotinylated-CD4 and CD8 antibodies (GK1.5 and 53–6.7, respectively [eBioscience] and streptavidin MACS beads (Miltenyi Biotec). DP thymocytes (CD4$^+$CD8$^+$) were obtained by sorting of whole thymocytes using FITC-CD8 (53–6.7) and PE/Cy7-CD4 (GK1.5) antibodies (eBioscience) or PE-CD4 (GK1.5) and FITC-CD8 (53–6.7) antibodies (BioLegend). Sorting was performed on a FACSVantage (BD) and the purity of cells after double sorting was >95%. Lymph node T cells were isolated as previously described (Jackson and Krangel, 2005).

In vitro survival assay. Sorted DP thymocytes (10^5) were cultured in 200 µl RPMI 1640 medium containing 10% FBS, 55 µM 2-mercaptoethanol, 2 mM L-glutamine, 100 U/ml penicillin, and 0.1 mg/ml streptomycin for varying times in the presence of 10 ng/ml mouse recombinant IL-7 (R&D Systems). Apoptosis was measured by Annexin V and 7-aminoactinomycin D staining using the Annexin V-PE kit (BD) according to the manufacturer's instructions.

ChIP. For immunoprecipitation using anti-trimethylated H3K4 (Millipore 04–745) or control rabbit IgG (ab-105-c; R&D Systems), chromatin was prepared without formaldehyde cross-linking and was immunoprecipitated exactly as previously described (Hao and Krangel, 2011). Immunoprecipitated and input samples were quantified by real-time PCR using a Roche LightCycler and a FastStart DNA Master Syber Green I kit (Roche). PCR conditions were as follows: 5 min at 95°C followed by 45 cycles of 1 s at 95°C, 5 s at 62°C, 7 s at 72°C. Analysis of *B2m* was used to normalize ratios of bound/input in different samples. Primers sequences are provided in Table S1.

For immunoprecipitation using anti-RNA pol II (Millipore; 05–623) or control rabbit IgG (R&D Systems; ab-105-c), 1×10^7 cells were subjected to cross-linking by incubation for 10 min on ice in 10 ml of RPMI 1640 containing 10% FBS and 1% formaldehyde. The reaction was stopped by addition of glycine to 0.125 M and incubation for 5 min at 23°C. Cells were then washed in PBS and lysed by incubation for 10 min on ice in 1 ml of 5 mM PIPES, pH 8.0, 85 mM KCl, 0.5% NP-40, 0.1 mM PMSF, and 0.1 mM benzamidine. Nuclei were pelleted and lysed by resuspension in 0.3 ml 50 mM Tris-HCl, pH 8.0, 10 mM EDTA, and 1% SDS. Chromatin was then pelleted through 8 M urea by centrifugation at 30,000 rpm for 16 h at 10°C in a Beckman SW 40Ti rotor. After centrifugation, pelleted chromatin was resuspended in 10 mM Tris, pH 8.0, 1 mM EDTA, 5% glycerol, was dialyzed overnight at 4°C against the same buffer. The volume was then adjusted to 1 ml and the suspension was sonicated using a Model 550 Sonic Dismembrator (Thermo Fisher Scientific), alternating 15 s on and 20 s off for 10 cycles with the sample immersed in an ice/water bath. Chromosomal DNA was reduced to an average size of 300–500 bp, as determined by agarose gel electrophoresis. Sonicated chromatin was precleared with Protein A-Sepharose/salmon sperm DNA slurry (Millipore), incubated overnight at 4°C with anti-RNA pol II or control rabbit IgG, and was subsequently incubated for 1 h with Protein A–Sepharose/salmon sperm DNA slurry. Immunoprecipitated DNA was then purified after vigorous washing of immunoprecipitates and reversal of cross-links by overnight incubation at 60°C. Immunoprecipitated and input samples were quantified by real-time PCR using a Roche LightCycler 480 and a QuantiFast SYBRgreen kit (QIAGEN). PCR conditions were as follows: 5 min at 95°C followed by 45 cycles of 10 s at 95°C, 30 s at 62°C.

ChIP-seq. For ChIP-seq using anti-SATB1 (Abcam; ab109122), 4×10^7 C57BL/6 thymocytes were freshly prepared and washed with PBS containing 0.5 mM PMSF and were subjected to cross-linking by incubation for 10 min in 5 mM Hepes, pH 7.5, 10 mM NaCl, 0.1 mM EDTA, 0.05 mM EGTA, 1% formaldehyde at 23°C. The reaction was stopped by addition of glycine to 0.125 M. Cells were then immediately washed in ice-cold PBS containing 0.5 mM PMSF and lysed by incubation for 10 min on ice in 1 ml of 50 mM Hepes, pH 7.5, 140 mM NaCl, 1 mM EDTA, 10% Glycerol, 0.5% NP-40, 0.25% TritonX-100 containing protease inhibitor (Roche). Nuclei were pelleted and lysed by resuspending in 10 mM Tris-HCl, pH 8.0, 200 mM NaCl, 1 mM EDTA, and 0.5 mM EGTA containing protease inhibitor (Roche). Pelleted chromatin was resuspended in 400 µl of 10 mM Tris, pH 8.0, 300 mM NaCl, 1 mM EDTA, 0.5 mM EGTA, 1% TritonX-100, 0.1% sodium deoxycholate and 0.5% N-laurylsarcosine, and was sonicated using a model XL2000 ultrasonic cell disruptor (MICROSON) so that relatively large fragments (1–10 kbp) were included. Sonicated chromatin was incubated overnight at 4°C with anti-SATB1 antibody that was preconjugated

with Magnet beads (Dynabeads). Immunoprecipitated DNA was then purified after vigorous washing of immunoprecipitates and reversal of cross-links by overnight incubation at 65°C in 50 mM Tris, pH 8.0, 10 mM EDTA, and 1% SDS. Input DNA and ChIP DNA (10–20 ng) were subjected to sonication (Bioruptor; UCD-200) at medium power for 20 min, alternating 30 s on and 30 s off. Library construction was conducted as follows: (1) End repair by T4 DNA polymerase, Klenow DNA polymerase and T4 kinase; (2) A-tailing by Klenow exo-; (3) Adaptor ligation using Illimina TruSeq adaptors (Illumina) and T4 DNA ligase; (4) 15 cycles of PCR amplification by AccuPrime DNA Taq polymerase (Invitrogen) and TruSeq primers; (5) purification of final products by size selection (200–1,000 bp) using SPRI beads (Thermo Fisher Scientific). The ChIP-sequencing was performed by the UC Berkeley sequence facility. The Gene Expression Omnibus accession no. for the SATB1 ChIP-seq dataset is GSE66248.

Quantitative RT-PCR. Total RNA was isolated using TRIzol (Invitrogen) according to the manufacturer's instructions, and cDNA was synthesized using oligo dT primers and SuperScript III (Invitrogen). PCR was performed using an iCycler MyiQ Real-Time PCR Detection System (Bio-Rad Laboratories) and SYBR Green PCR core reagents (Applied Biosystems). PCR conditions (for *Rag1*, *Rag2*, and *Actb*) were as follows: 95°C for 10 min, followed by 35 cycles of 95°C for 15 s and 60°C for 45 s. Relative expression levels of target genes were normalized to the value for *Actb* in each sample. Primers sequences are provided in Table S1.

***Tcra* recombination.** To quantify *Tcra* coding joints, thymocytes were lysed by overnight incubation at 37°C in 10 mM Tris-HCl, pH 8.0, 150 mM NaCl, 10 mM EDTA, 0.4% SDS, 0.1 mg/ml proteinase K, and genomic DNA was prepared by phenol/chloroform extraction and ethanol precipitation. Quantitative real-time PCR with Vα and Jα-specific primers was performed using a Roche LightCycler and a FastStart DNA Master Syber Green I kit (Roche). PCR conditions were as described above.

To quantify Jα signal ends, genomic DNA was linker-ligated as described (McMurry et al., 1997) and linker-ligated DNA was used to amplify signal ends by 'touchdown' PCR (Jackson et al., 2005). Conditions for *Cd14* amplification were: 94°C for 5 min, followed by 25 cycles of 94°C for 30 s, 62°C for 30 s and 72°C for 1 min, and a 10-min extension at 72°C. Amplicons were separated by agarose gel electrophoresis and analyzed by Southern blot with ^{32}P-labeled oligonucleotide probes. Primers and probes were described previously (Seitan et al., 2011).

To evaluate relative Jα usage in *Tcra* transcripts, total RNA was extracted from whole thymus using TRIzol (Invitrogen) according to the manufacturer's instructions. Contaminating genomic DNA was removed by incubation with 1 U DNaseI (New England Biolabs) for 10 min at 37°C. cDNA was synthesized using SuperScript reverse transcriptase and oligo$(dT)_{20}$ according to the manufacturer's instructions. Jα usage was determined in Vα8 *Tcra* transcripts as previously described (Hawwari et al., 2005).

3C. This technique was performed with some modifications to a previously described protocol (Hagège et al., 2007). 1×10^7 cells were subjected to cross-linking by incubation for 10 min on ice in 10 ml of RPMI-1640 containing 10% FBS and 2% formaldehyde. The reaction was stopped by addition of glycine to 0.125 M and incubation for 5 min at 23°C. Cells were then washed in PBS and lysed by incubation for 10 min on ice in 5 ml of 10 mM Tris, pH 8.0, 10 mM NaCl, 0.2% NP-40, 0.1 mM benzamidine, and 0.1 mM PMSF. Nuclei were pelleted, washed once with PBS, and lysed by incubation for 1 h at 37°C in 0.5 ml of 1× NEB II or NEB III digestion buffer (New England Biolabs) containing 0.3% SDS. Triton-X100 was then added to a final concentration of 2% and incubation was continued for an additional 1 h at 37°C. Chromatin was then digested by addition of 200 U BglII or HindIII for overnight incubation at 37°C, followed by a second addition of 200 U of enzyme for an additional 8 h incubation at 37°C. Digested chromatin was then sedimented through 8 M urea by centrifugation at 35,000 rpm for 16 h at 10°C in a Beckman SW 40Ti rotor. After centrifugation, the digested chromatin (0.5 ml of gel and liquid) was diluted and resuspended in 2 ml H_2O, dialyzed overnight at 4°C against 30 mM Tris, pH 7.4, 10 mM $MgCl_2$, diluted to 7 ml in 30 mM Tris, pH 7.4, 10 mM $MgCl_2$, 1 mM DTT, and 0.1 mM ATP, and was ligated by addition of 4,000 U T4 DNA ligase for overnight incubation at 16°C. Ligated chromatin was incubated overnight at 60°C to reverse cross-links and DNA was purified by extraction with phenol/chloroform and ethanol precipitation.

Ligation products were quantified by TaqMan quantitative real-time PCR (Roche) using a Roche LightCycler 480 and PCR conditions as follows: 5 min at 95°C followed by 45 cycles of 10 s at 95°C and 30 s at 62°C. To generate ligation product standards, 10 µg of BAC RP23-325I3 was digested at 37°C overnight with 50 U HindIII or BglII, after which DNA was purified by phenol/chloroform extraction and ethanol precipitation, and then ligated overnight at 16°C in a 200 µl reaction containing 40 U T4 DNA ligase. Purified, ligated DNA was serially diluted in 10-fold increments from a 2 ng/µl stock to generate the standard curve.

Digestion efficiencies of different experimental samples were 90–94% as determined by quantitative real-time PCR in which yields of several amplicons that span HindIII or BglII sites were compared with yields of neighboring amplicons that were not disrupted by digestion. Normalization of 3C PCR signals from different samples was accomplished by setting the nonspecific interaction of the bait fragment with one of its nearest neighbor fragments equal to one in each sample. Primer and probe sequences are provided in Table S1.

FAIRE. FAIRE was performed essentially as previously described (Giresi et al., 2007) except that quantitative real-time PCR was used to evaluate enrichment of sequences in DNA purified from formaldehyde-cross-linked as compared with uncrosslinked samples. Primer sequences are provided in Table S1.

Luciferase. VL3-3M2 cells were provided by S. Sarafova (Davidson College, Davidson, NC) and were cultured in RPMI-1640 supplemented with 10% fetal bovine serum, 100 U/ml penicillin, 100 µg/ml streptomycin, 55 µM 2-mercaptoethanol, 2 mM L-glutamine, and 25 mM Hepes, pH 7.0. Approximately 3×10^5 cells were transfected with versions of the pXPG firefly luciferase reporter plasmid (Bert et al., 2000) containing the Rag1 or Rag2 promoter and different anti-silencer region or control DNA fragments. In brief, 1 µg of each construct was cotransfected with 100 ng of plasmid expressing Renilla luciferase using the Superfect transfection reagent (QIAGEN). Cells were cultured for 48 h in 0.5 ml of medium in a 24-well plate and were then harvested to assay for luciferase activity using an Infinite F200 Tecan plate luminometer and a Dual-Luciferase Reporter Assay kit (Promega) according to the manufacturer's instructions.

Online supplemental material. Fig. S1 shows normal DN-to-DP transition in SATB1-deficient thymocytes. Table S1 lists oligonucleotides used as PCR primers and probes. Online supplemental material is available at http://www.jem.org/cgi/content/full/jem.20142207/DC1.

We thank Lynn Martinek, Nancy Martin, and Mike Cook of the Duke Cancer Institute Flow Cytometry Facility for help with cell sorting and analysis, Kingshuk Roy Choudhury for advice on statistical analysis, and Eugene Oltz for critical reading of the manuscript.

This work was supported by National Institutes of Health grants R37 GM10452 (to M.S.K.) and R37 CA39681 (to T.K.S.), by a Grant-in-Aid for Scientific Research (S) and for Scientific Research on Priority Areas (to I.T.), and by grant JSPS KAKENHI 24390121 and a Leukemia and Lymphoma Society Scholar Award (to M.K.).

The authors declare no competing financial interests.

Submitted: 25 November 2014
Accepted: 12 March 2015

REFERENCES

Ahlfors, H., A. Limaye, L.L. Elo, S. Tuomela, M. Burute, K.V. Gottimukkala, D. Notani, O. Rasool, S. Galande, and R. Lahesmaa. 2010. SATB1 dictates expression of multiple genes including IL-5 involved in human T helper cell differentiation. *Blood*. 116:1443–1453. http://dx.doi.org/10.1182/blood-2009-11-252205

Alvarez, J.D., D.H. Yasui, H. Niida, T. Joh, D.Y. Loh, and T. Kohwi-Shigematsu. 2000. The MAR-binding protein SATB1 orchestrates temporal and spatial

expression of multiple genes during T-cell development. *Genes Dev.* 14:521–535.

Balamotis, M.A., N. Tamberg, Y.J. Woo, J. Li, B. Davy, T. Kohwi-Shigematsu, and Y. Kohwi. 2012. Satb1 ablation alters temporal expression of immediate early genes and reduces dendritic spine density during postnatal brain development. *Mol. Cell. Biol.* 32:333–347. http://dx.doi.org/10.1128/MCB.05917-11

Bert, A.G., J. Burrows, C.S. Osborne, and P.N. Cockerill. 2000. Generation of an improved luciferase reporter gene plasmid that employs a novel mechanism for high-copy replication. *Plasmid*. 44:173–182. http://dx.doi.org/10.1006/plas.2000.1474

Beyer, M., Y. Thabet, R.U. Müller, T. Sadlon, S. Classen, K. Lahl, S. Basu, X. Zhou, S.L. Bailey-Bucktrout, W. Krebs, et al. 2011. Repression of the genome organizer SATB1 in regulatory T cells is required for suppressive function and inhibition of effector differentiation. *Nat. Immunol.* 12: 898–907. http://dx.doi.org/10.1038/ni.2084

Bulger, M., and M. Groudine. 2011. Functional and mechanistic diversity of distal transcription enhancers. *Cell*. 144:327–339. http://dx.doi.org/10.1016/j.cell.2011.01.024

Cai, S., H.J. Han, and T. Kohwi-Shigematsu. 2003. Tissue-specific nuclear architecture and gene expression regulated by SATB1. *Nat. Genet.* 34:42–51. http://dx.doi.org/10.1038/ng1146

Cai, S., C.C. Lee, and T. Kohwi-Shigematsu. 2006. SATB1 packages densely looped, transcriptionally active chromatin for coordinated expression of cytokine genes. *Nat. Genet.* 38:1278–1288. http://dx.doi.org/10.1038/ng1913

Calo, E., and J. Wysocka. 2013. Modification of enhancer chromatin: what, how, and why? *Mol. Cell.* 49:825–837. http://dx.doi.org/10.1016/j.molcel.2013.01.038

Cisse, I.I., I. Izeddin, S.Z. Causse, L. Boudarene, A. Senecal, L. Muresan, C. Dugast-Darzacq, B. Hajj, M. Dahan, and X. Darzacq. 2013. Real-time dynamics of RNA polymerase II clustering in live human cells. *Science*. 341:664–667. http://dx.doi.org/10.1126/science.1239053

Cook, P.R. 1999. The organization of replication and transcription. *Science*. 284:1790–1795. http://dx.doi.org/10.1126/science.284.5421.1790

de Boer, J., A. Williams, G. Skavdis, N. Harker, M. Coles, M. Tolaini, T. Norton, K. Williams, K. Roderick, A.J. Potocnik, and D. Kioussis. 2003. Transgenic mice with hematopoietic and lymphoid specific expression of Cre. *Eur. J. Immunol.* 33:314–325. http://dx.doi.org/10.1002/immu.200310005

Dekker, J., K. Rippe, M. Dekker, and N. Kleckner. 2002. Capturing chromosome conformation. *Science*. 295:1306–1311. http://dx.doi.org/10.1126/science.1067799

Dickinson, L.A., T. Joh, Y. Kohwi, and T. Kohwi-Shigematsu. 1992. A tissue-specific MAR/SAR DNA-binding protein with unusual binding site recognition. *Cell*. 70:631–645. http://dx.doi.org/10.1016/0092-8674(92)90432-C

Domen, J., K.L. Gandy, and I.L. Weissman. 1998. Systemic overexpression of BCL-2 in the hematopoietic system protects transgenic mice from the consequences of lethal irradiation. *Blood*. 91:2272–2282.

Fessing, M.Y., A.N. Mardaryev, M.R. Gdula, A.A. Sharov, T.Y. Sharova, V. Rapisarda, K.B. Gordon, A.D. Smorodchenko, K. Poterlowicz, G. Ferone, et al. 2011. p63 regulates Satb1 to control tissue-specific chromatin remodeling during development of the epidermis. *J. Cell Biol.* 194: 825–839. http://dx.doi.org/10.1083/jcb.201101148

Ghamari, A., M.P. van de Corput, S. Thongjuea, W.A. van Cappellen, W. van Ijcken, J. van Haren, E. Soler, D. Eick, B. Lenhard, and F.G. Grosveld. 2013. In vivo live imaging of RNA polymerase II transcription factories in primary cells. *Genes Dev.* 27:767–777. http://dx.doi.org/10.1101/gad.216200.113

Gibcus, J.H., and J. Dekker. 2013. The hierarchy of the 3D genome. *Mol. Cell.* 49:773–782. http://dx.doi.org/10.1016/j.molcel.2013.02.011

Giresi, P.G., J. Kim, R.M. McDaniell, V.R. Iyer, and J.D. Lieb. 2007. FAIRE (Formaldehyde-Assisted Isolation of Regulatory Elements) isolates active regulatory elements from human chromatin. *Genome Res.* 17:877–885. http://dx.doi.org/10.1101/gr.5533506

Guo, J., A. Hawwari, H. Li, Z. Sun, S.K. Mahanta, D.R. Littman, M.S. Krangel, and Y.W. He. 2002. Regulation of the TCRalpha repertoire by the survival window of CD4(+)CD8(+) thymocytes. *Nat. Immunol.* 3:469–476. http://dx.doi.org/10.1038/ni791

Hagège, H., P. Klous, C. Braem, E. Splinter, J. Dekker, G. Cathala, W. de Laat, and T. Forné. 2007. Quantitative analysis of chromosome conformation capture assays (3C-qPCR). *Nat. Protoc.* 2:1722–1733. http://dx.doi.org/10.1038/nprot.2007.243

Han, H.J., J. Russo, Y. Kohwi, and T. Kohwi-Shigematsu. 2008. SATB1 reprogrammes gene expression to promote breast tumour growth and metastasis. *Nature*. 452:187–193. http://dx.doi.org/10.1038/nature06781

Hao, B., and M.S. Krangel. 2011. Long-distance regulation of fetal V(δ) gene segment TRDV4 by the Tcrd enhancer. *J. Immunol.* 187:2484–2491. http://dx.doi.org/10.4049/jimmunol.1100468

Hawwari, A., C. Bock, and M.S. Krangel. 2005. Regulation of T cell receptor α gene assembly by a complex hierarchy of germline Jalpha promoters. *Nat. Immunol.* 6:481–489. http://dx.doi.org/10.1038/ni1189

Hsu, L.Y., J. Lauring, H.E. Liang, S. Greenbaum, D. Cado, Y. Zhuang, and M.S. Schlissel. 2003. A conserved transcriptional enhancer regulates RAG gene expression in developing B cells. *Immunity*. 19:105–117. http://dx.doi.org/10.1016/S1074-7613(03)00181-X

Jackson, A.M., and M.S. Krangel. 2005. Allele-specific regulation of TCR β variable gene segment chromatin structure. *J. Immunol.* 175:5186–5191. http://dx.doi.org/10.4049/jimmunol.175.8.5186

Jackson, A., H.D. Kondilis, B. Khor, B.P. Sleckman, and M.S. Krangel. 2005. Regulation of T cell receptor β allelic exclusion at a level beyond accessibility. *Nat. Immunol.* 6:189–197. http://dx.doi.org/10.1038/ni1157

Jhunjhunwala, S., M.C. van Zelm, M.M. Peak, and C. Murre. 2009. Chromatin architecture and the generation of antigen receptor diversity. *Cell.* 138:435–448. http://dx.doi.org/10.1016/j.cell.2009.07.016

Kim, T.K., M. Hemberg, J.M. Gray, A.M. Costa, D.M. Bear, J. Wu, D.A. Harmin, M. Laptewicz, K. Barbara-Haley, S. Kuersten, et al. 2010. Widespread transcription at neuronal activity-regulated enhancers. *Nature*. 465:182–187. http://dx.doi.org/10.1038/nature09033

Koch, F., R. Fenouil, M. Gut, P. Cauchy, T.K. Albert, J. Zacarias-Cabeza, S. Spicuglia, A.L. de la Chapelle, M. Heidemann, C. Hintermair, et al. 2011. Transcription initiation platforms and GTF recruitment at tissue-specific enhancers and promoters. *Nat. Struct. Mol. Biol.* 18:956–963. http://dx.doi.org/10.1038/nsmb.2085

Kohwi-Shigematsu, T., K. Poterlowicz, E. Ordinario, H.J. Han, V.A. Botchkarev, and Y. Kohwi. 2013. Genome organizing function of SATB1 in tumor progression. *Semin. Cancer Biol.* 23:72–79. http://dx.doi.org/10.1016/j.semcancer.2012.06.009

Krangel, M.S. 2009. Mechanics of T cell receptor gene rearrangement. *Curr. Opin. Immunol.* 21:133–139. http://dx.doi.org/10.1016/j.coi.2009.03.009

Kumar, P.P., P.K. Purbey, C.K. Sinha, D. Notani, A. Limaye, R.S. Jayani, and S. Galande. 2006. Phosphorylation of SATB1, a global gene regulator, acts as a molecular switch regulating its transcriptional activity in vivo. *Mol. Cell.* 22:231–243. http://dx.doi.org/10.1016/j.molcel.2006.03.010

Kumar, P.P., O. Bischof, P.K. Purbey, D. Notani, H. Urlaub, A. Dejean, and S. Galande. 2007. Functional interaction between PML and SATB1 regulates chromatin-loop architecture and transcription of the MHC class I locus. *Nat. Cell Biol.* 9:45–56. http://dx.doi.org/10.1038/ncb1516

Kuo, T.C., and M.S. Schlissel. 2009. Mechanisms controlling expression of the RAG locus during lymphocyte development. *Curr. Opin. Immunol.* 21:173–178. http://dx.doi.org/10.1016/j.coi.2009.03.008

Li, W., D. Notani, Q. Ma, B. Tanasa, E. Nunez, A.Y. Chen, D. Merkurjev, J. Zhang, K. Ohgi, X. Song, et al. 2013. Functional roles of enhancer RNAs for oestrogen-dependent transcriptional activation. *Nature*. 498:516–520. http://dx.doi.org/10.1038/nature12210

Lund, R., H. Ahlfors, E. Kainonen, A.M. Lahesmaa, C. Dixon, and R. Lahesmaa. 2005. Identification of genes involved in the initiation of human Th1 or Th2 cell commitment. *Eur. J. Immunol.* 35:3307–3319. http://dx.doi.org/10.1002/eji.200526079

McMurry, M.T., C. Hernandez-Munain, P. Lauzurica, and M.S. Krangel. 1997. Enhancer control of local accessibility to V(D)J recombinase. *Mol. Cell. Biol.* 17:4553–4561.

Merkenschlager, M., and D.T. Odom. 2013. CTCF and cohesin: linking gene regulatory elements with their targets. *Cell.* 152:1285–1297. http://dx.doi.org/10.1016/j.cell.2013.02.029

Monroe, R.J., F. Chen, R. Ferrini, L. Davidson, and F.W. Alt. 1999. RAG2 is regulated differentially in B and T cells by elements 5′ of the

promoter. *Proc. Natl. Acad. Sci. USA*. 96:12713–12718. http://dx.doi.org/10.1073/pnas.96.22.12713

Natoli, G., and J.C. Andrau. 2012. Noncoding transcription at enhancers: general principles and functional models. *Annu. Rev. Genet*. 46:1–19. http://dx.doi.org/10.1146/annurev-genet-110711-155459

Notani, D., K.P. Gottimukkala, R.S. Jayani, A.S. Limaye, M.V. Damle, S. Mehta, P.K. Purbey, J. Joseph, and S. Galande. 2010. Global regulator SATB1 recruits beta-catenin and regulates T(H)2 differentiation in Wnt-dependent manner. *PLoS Biol*. 8:e1000296. http://dx.doi.org/10.1371/journal.pbio.1000296

Rosenbloom, K.R., C.A. Sloan, V.S. Malladi, T.R. Dreszer, K. Learned, V.M. Kirkup, M.C. Wong, M. Maddren, R. Fang, S.G. Heitner, et al. 2013. ENCODE data in the UCSC Genome Browser: year 5 update. *Nucleic Acids Res*. 41(D1):D56–D63. http://dx.doi.org/10.1093/nar/gks1172

Satoh, Y., T. Yokota, T. Sudo, M. Kondo, A. Lai, P.W. Kincade, T. Kouro, R. Iida, K. Kokame, T. Miyata, et al. 2013. The Satb1 protein directs hematopoietic stem cell differentiation toward lymphoid lineages. *Immunity*. 38:1105–1115. http://dx.doi.org/10.1016/j.immuni.2013.05.014

Savarese, F., A. Davila, R. Nechanitzky, I. De-La Rosa-Velazquez, C.F. Pereira, R. Engelke, K. Takahashi, T. Jenuwein, T. Kohwi-Shigematsu, A.G. Fisher, et al.. 2009. Satb1 and Satb2 regulate embryonic stem cell differentiation and Nanog expression. *Genes Dev*. 23:2625–2638. http://dx.doi.org/10.1101/gad.1815709

Schatz, D.G., and P.C. Swanson. 2011. V(D)J recombination: mechanisms of initiation. *Annu. Rev. Genet*. 45:167–202. http://dx.doi.org/10.1146/annurev-genet-110410-132552

Seitan, V.C., B. Hao, K. Tachibana-Konwalski, T. Lavagnolli, H. Mira-Bontenbal, K.E. Brown, G. Teng, T. Carroll, A. Terry, K. Horan, et al. 2011. A role for cohesin in T-cell-receptor rearrangement and thymocyte differentiation. *Nature*. 476:467–471. http://dx.doi.org/10.1038/nature10312

Shih, H.Y., and M.S. Krangel. 2013. Chromatin architecture, CCCTC-binding factor, and V(D)J recombination: managing long-distance relationships at antigen receptor loci. *J. Immunol*. 190:4915–4921. http://dx.doi.org/10.4049/jimmunol.1300218

Skowronska-Krawczyk, D., Q. Ma, M. Schwartz, K. Scully, W. Li, Z. Liu, H. Taylor, J. Tollkuhn, K.A. Ohgi, D. Notani, et al. 2014. Required enhancer-matrin-3 network interactions for a homeodomain transcription program. *Nature*. 514:257–261. http://dx.doi.org/10.1038/nature13573

Stamatoyannopoulos, J.A., M. Snyder, R. Hardison, B. Ren, T. Gingeras, D.M. Gilbert, M. Groudine, M. Bender, R. Kaul, T. Canfield, et al. Mouse ENCODE Consortium. 2012. An encyclopedia of mouse DNA elements (Mouse ENCODE). *Genome Biol*. 13:418. http://dx.doi.org/10.1186/gb-2012-13-8-418

Will, B., T.O. Vogler, B. Bartholdy, F. Garrett-Bakelman, J. Mayer, L. Barreyro, A. Pandolfi, T.I. Todorova, U.C. Okoye-Okafor, R.F. Stanley, et al. 2013. Satb1 regulates the self-renewal of hematopoietic stem cells by promoting quiescence and repressing differentiation commitment. *Nat. Immunol*. 14:437–445. http://dx.doi.org/10.1038/ni.2572

Yannoutsos, N., P. Wilson, W. Yu, H.T. Chen, A. Nussenzweig, H. Petrie, and M.C. Nussenzweig. 2001. The role of recombination activating gene (RAG) reinduction in thymocyte development in vivo. *J. Exp. Med*. 194:471–480. http://dx.doi.org/10.1084/jem.194.4.471

Yannoutsos, N., V. Barreto, Z. Misulovin, A. Gazumyan, W. Yu, N. Rajewsky, B.R. Peixoto, T. Eisenreich, and M.C. Nussenzweig. 2004. A cis element in the recombination activating gene locus regulates gene expression by counteracting a distant silencer. *Nat. Immunol*. 5:443–450. http://dx.doi.org/10.1038/ni1053

Yasui, D., M. Miyano, S. Cai, P. Varga-Weisz, and T. Kohwi-Shigematsu. 2002. SATB1 targets chromatin remodelling to regulate genes over long distances. *Nature*. 419:641–645. http://dx.doi.org/10.1038/nature01084

Yu, W., Z. Misulovin, H. Suh, R.R. Hardy, M. Jankovic, N. Yannoutsos, and M.C. Nussenzweig. 1999. Coordinate regulation of RAG1 and RAG2 by cell type-specific DNA elements 5′ of RAG2. *Science*. 285:1080–1084. http://dx.doi.org/10.1126/science.285.5430.1080

Zhang, W., C.L. Sommers, D.N. Burshtyn, C.C. Stebbins, J.B. DeJarnette, R.P. Trible, A. Grinberg, H.C. Tsay, H.M. Jacobs, C.M. Kessler, et al. 1999. Essential role of LAT in T cell development. *Immunity*. 10:323–332. http://dx.doi.org/10.1016/S1074-7613(00)80032-1